Nup107 is a crucial regulator of torso-mediated metamorphic transition in *Drosophila melanogaster*

Jyotsna Kawadkar[1*], Pradyumna Ajit Joshi[1] and Ram Kumar Mishra[1*]

Department of Biological Sciences, Indian Institute of Science Education and Research (IISER) Bhopal

Bhopal, Madhya Pradesh, India

* Corresponding author: rkmishra@iiserb.ac.in, @rkmisrb, jyotsna19@iiserb.ac.in

Abstract

Nuclear pore complexes (NPCs), composed of nucleoporins (Nups), affect nucleocytoplasmic transport, thus influencing cell division and gene regulation. Nup107 subcomplex members have been studied in housekeeping functions, diseases, and developmental disorders.

We report a unique regulatory function for Nup107 in metamorphic transition during *Drosophila* development. RNAi-mediated *Nup107* depleted larvae were arrested in the third-instar larval stage and completely ceased to pupariate. The pupariation defect is primarily due to inhibited nuclear translocation and transcriptional activation by EcR. We unequivocally demonstrate the involvement of Nup107 in the transcription of the *Halloween* genes, modulating ecdysone biosynthesis and the EcR pathway activation. The regulation of EcR-mediated metamorphosis by the receptor tyrosine kinase, *torso*, is well documented. Accordingly, overexpression of the *torso* and MAP-kinase pathway activator, ras^{V12}, in the *Nup107* depletion background rescues the phenotypes, implying that Nup107 is an epistatic regulator of Torso-mediated activation of EcR signaling during metamorphosis.

Key words: Nup107, Torso, Ecdysone receptor, Metamorphosis, Prothoracicotropic hormone, Y-complex, Halloween genes

Introduction

The multi-protein assembly of nucleoporins (Nups) constitutes nuclear pore complexes (NPCs). In eukaryotic cells, NPCs serve as molecular conduits for the trafficking of proteins and RNAs between the nucleus and the cytoplasm. The NPC composition was revealed from proteomic analyses conducted in yeasts and vertebrates, have contributed to our understanding, revealing that Approximately 30 distinct Nups are arranged in sub-structures and are distributed on different faces of NPCs (Cronshaw et al., 2002; Rout et al., 2000). The substructures are the outer cytoplasmic and inner nuclear rings, which surround a central inner ring called the scaffold ring, primarily aiding in the process of nucleocytoplasmic transport (Lin & Hoelz, 2019).

The largest Nup107 sub-complex, also called the Y-complex, is symmetrically located on both sides of the nuclear membrane. In metazoans, the Y-complex is composed of ten distinct Nups (ELYS, Nup160, Nup133, Nup107, Nup96, Nup85, Nup43, Nup37, Sec13, and Seh1). ELYS is a sub-stoichiometric Y-complex member and is present only on the nucleoplasmic side (D'Angelo & Hetzer, 2008; Morchoisne-Bolhy et al., 2015). Nup107, along with Nup133, forms the stalk of the Y-complex and is critically required for the Y-complex stability. The Nup107 complex plays a pivotal role in facilitating ELYS-coordinated post-mitotic NPC assembly (Boehmer et al., 2003; Walther et al., 2003) and messenger RNA (mRNA) export (Bai et al., 2004). Additionally, The Nup107 complex members actively participate in mitosis, contributing to the regulation of kinetochore-microtubule polymerization (Mishra et al., 2010; Zuccolo et al., 2007). The multitude of cellular processes where the Y-complex performs vital functions suggests it to be a central component in maintaining cellular homeostasis.

As a stable constituent of NPC, many Nups, including the members of the Y-complex, associate with chromatin and exert transcriptional regulation. Notably, interactions between active genes and Nups occurring predominantly within the nucleoplasm have been reported for dynamic Nups such as Nup98, ELYS, and Sec13 (Capelson, Liang, et al., 2010; Kalverda et al., 2010; Kuhn et al., 2019). In *Drosophila*, the dual nucleoporin, ELYS, governs the development, and ELYS RNAi-induced developmental defects are

due to the reactivation of the Dorsal (NF-κB) pathway even during the late larval stages (Mehta et al., 2020).

Nup107 is associated with actively transcribing genes at the nuclear periphery (Gozalo et al., 2020). The disruption of Nup107 in zebrafish embryos leads to significant developmental anomalies, including the absence of the pharyngeal skeleton (Zheng et al., 2012). Moreover, the biallelic Nup107 mutations (D157Y and D831A) correlate well with clinical conditions such as microcephaly and steroid-resistant nephrotic Syndrome (Miyake et al., 2015). In *Drosophila*, Nup107 co-localizes with Lamin during meiotic division, and Nup107 depletion perturbs lamin localization, leading to a higher frequency of cytokinesis failure during male meiosis (Hayashi et al., 2016). Nup107 influences the regulation of cell fate in aged and transformed cells by modulating EGFR signaling and the nuclear trafficking of ERK protein (Kim et al., 2010).

Drosophila undergoes elaborate metamorphosis initiated by the neuropeptide prothoracicotropic hormone (PTTH) (Rewitz et al., 2013). Bilateral neurons projecting into the prothoracic gland (PG), when stimulated by the PTTH, induce Ecdysone production, which is subsequently released into the circulatory system for conversion by peripheral tissues into its active form, 20-hydroxyecdysone (20E) (Johnson et al., 2013; McBrayer et al., 2007; Shimell et al., 2018). The 20E binds to the ecdysone receptor, and the whole complex translocates into the nucleus and binds to chromatin to activate ecdysone inducible genes (Johnston et al., 2011; Kozlova & Thummel, 2002; Tennessen & Thummel, 2011). In the prothoracic gland, the primary neuroendocrine organ, PTTH signals through the receptor tyrosine kinase (RTK), Torso. The Torso-dependent activation of the MAP-kinase pathway is responsible for the production and release of ecdysone hormone. However, ecdysone synthesis can also be regulated by the EGFR pathway (Cruz et al., 2020; Yamanaka et al., 2013). While Nup107 modulates EGFR pathway activation, the involvement of EGFR and torso pathways in ecdysone-dependent metamorphosis is undeniable. We dissect the involvement of Nup107 in Torso-mediated signaling and underlying mechanisms during *Drosophila* metamorphosis.

In a reverse genetic RNAi screening for Nup107 complex members, we noted that *Nup107* RNAi induces a significant developmental arrest at the third instar larval stage. Further analysis revealed that the Ecdysone Receptor (EcR) signaling pathway is perturbed, and EcR fails to translocate into the nucleus in *Nup107* knockdown. The failure of the EcR nuclear localization upon *Nup107* depletion is due to significantly reduced levels of the ecdysone hormone during the late third instar larval stage. Interestingly, overexpression of the *torso* and the ras^{V12} in *Nup107* depleted larvae rescued the developmental arrest and subsequently initiated pupation. We propose that Nup107, an epistatic regulator of torso-pathway activation in the PG, enables ecdysone surge for efficient metamorphic transition.

Results

Nup107 is essential for larval to pupal metamorphic transition

Cell biological analyses in the mammalian cell culture system has shed light on critical regulatory roles of Nup107 in vertebrates. Yet its importance in development is poorly understood. In this context, we started the characterization of *Drosophila* Y-complex member Nup107 in greater detail. Utilizing RNAi lines ($Nup107^{KK}$ and $Nup107^{GD}$), we performed ubiquitous depletion through *Actin5C-GAL4*. Interestingly, *Nup107* depletion, leading to larvae arrest at the third instar stage, causing complete cessation of pupariation (120 h AEL, right panel, Figure 1A), was accompanied by an extension of larval feeding and growth periods. Quantitative assessment of *Nup107* transcript levels in the $Nup107^{GD}$ and $Nup107^{KK}$ RNAi lines suggested efficient *Nup107* knockdown (approximately 60-70%, Figure 1B). For further analyses, we generated polyclonal antibodies against the Nup107 amino-terminal antigenic fragment (amino acids 1–210; see methods for details). Purified anti-Nup107 polyclonal antibodies detected a band of approximately ~100 kDa in lysates prepared from the control larval brain complex. The intensity of this ~100 kDa band was significantly reduced in lysates prepared from organisms where *Nup107* was knocked down ubiquitously (Figure 1C) using *Actin5C-GAL4* driving *Nup107* RNAi (denoted as ubiquitous hereon). Further, the immunostaining with Nup107 antibodies identified a conserved and robust nuclear rim

staining pattern overlapping with mAb414 antibodies recognizing FG-nucleoporins (Figure S1A) and mRFP-tagged Nup107 expressed through its endogenous promoter (Figure S1B) in salivary gland tissues. These observations confirm the efficacy of *Nup107* knockdown and provide a handle to assess levels and localization of Nup107 in affected tissues. To further investigate the role of Nup107 in development, we generated a *Nup107* null mutant using CRISPR-Cas9-mediated gene editing. This comprehensive approach involving RNAi-mediated knockdown and CRISPR-Cas9 gene editing is expected to provide valuable insights into the significance of *Nup107* in *Drosophila* development. The gRNAs targeting regions close to the start and stop codon of the *nup107* gene generated knockout ($Nup107^{KO}$) mutants, which were confirmed by sequencing and PCR (Figures S2A and S2B). However, the $Nup107^{KO}$ mutants could not be used as the $Nup107^{KO}$ homozygous shows lethality at the embryonic stage. So, we carried out most of the analyses hereon with *Nup107* RNAi lines.

Nup107 **contributes significantly to ecdysone signaling**

The depletion of *Nup107* in *Drosophila* resulted in a distinct halt in growth and a developmental arrest at the third instar stage (Figure 1A). To discern the pathways affecting juvenile to adult developmental transition in *Drosophila*, we focused on levels of the sole insect steroid hormone, ecdysone.

We examined the localization of EcR in the late third instar salivary glands of both the control and *Nup107*-depleted larvae (using the $Nup107^{KK}$ line). Wild-type larvae exhibited normal EcR localization within the nucleus, but the nuclear translocation of EcR is perturbed in the *Nup107*-depleted larvae, with the bulk of the signal retained in the cytoplasm (Figures 2A and 2B). Quantitative analysis of EcR intensities in the cytoplasm and nucleus further established a significant decrease in EcR signals inside the nucleus when *Nup107* is depleted (Figure 2C). This observation suggests that the Nup107 is required for EcR nuclear localization to mediate critical larval to pupal developmental transition. Furthermore, we noticed that significantly smaller size salivary glands and the brain complex in *Nup107* depleted larvae (Figure S3).

Prompted by the cytoplasmic accumulation of EcR, we investigated whether the mRNA levels of ecdysone-inducible genes were affected. When 20E binds with EcR, the

activated EcR with enhanced affinity occupies the ecdysone response element (ERE) region in gene promoters. The ecdysone receptor is thought to function in a positive auto-regulatory loop, which may elevate EcR levels and sustain ecdysone signaling (Varghese & Cohen, 2007). Firstly, we examined the EcR transcript levels, revealing a reduction under *Nup107*-depletion conditions (Figure 2D). Subsequently, we measured the mRNA levels of known EcR target genes, *Eip75A* and *Eip74EF*, to find that the expression of each of these two target genes is reduced and correlates with *Nup107* knockdown levels (Figures 2E and 2F). Similar results were observed in the depletion of *Nup107* using the GD-based RNAi line (Figure S4). The defects observed during metamorphic transitions can be attributed to impaired ecdysone signaling upon *Nup107*-depletion, which prompted a closer examination of their regulatory relationship.

Nup107 **is dispensable for the nuclear import of EcR in the target tissue**

We established that the nuclear localization of EcR is impaired upon *Nup107* knockdown (see Figure 2B). Typically, EcR nuclear localization follows an intricate mechanism where 20E binding to EcR allows its nuclear translocation and subsequent activation of its target genes (Cronauer et al., 2007; Johnston et al., 2011; Lenaerts et al., 2019). Biosynthesis of ecdysone hormone from dietary cholesterol requires a group of P450 enzymes coded by the *Halloween* genes, is a prerequisite for EcR activation (Kannangara et al., 2021; Niwa & Niwa, 2014). Moreover, the involvement of nucleoporin, Nup358, in facilitating nuclear transport of Met juvenile hormone receptors is well documented (He et al., 2017). Consequently, we posited the hypothesis that Nup107 either disallows active 20E-EcR complex formation by affecting 20E biosynthesis in ubiquitous *Nup107* knockdown scenarios or directly regulates EcR nuclear translocation in the target tissue.

We chose salivary glands to address these hypotheses and depleted *Nup107* using salivary glands-specific *AB1-GAL4* and PG-specific *Phm-GAL4*. Surprisingly, in contrast to the ubiquitous knockdown of *Nup107*, nuclear localization of EcR remained unaffected in salivary gland-specific *Nup107* knockdown (Figures 3A, 3B, S5A and S5B). Interestingly, the PG-specific *Nup107* knockdown phenocopied ubiquitous *Nup107* knockdown induced EcR nuclear localization defects (Figures 3C and S5C).

Quantification of EcR signals from *Nup107* depleted late third instar salivary gland cells and comparison with control salivary glands indicates that the nuclear/cytoplasmic ratios are drastically reduced in case of PG-specific depletion but unaltered in salivary gland-specific *Nup107* depletion (Figures 3D and S5D). Consistent with these observations, expression levels of ecdysone-inducible genes *Eip75A* and *Eip74EF* were significantly reduced in PG-specific *Nup107* knockdown (Figures 3E, 3F, S5E and S5F). In accordance with unperturbed EcR nuclear translocation, salivary glands-specific depletion of *Nup107* yielded no discernible differences in larval growth and pupariation compared to the control (Figures S6A and S6C). However, the PG-specific knockdown induced an extended third instar stage lifespan (10-12 days after egg laying, Figures S6B and S6C). The observed decrease in ecdysone-inducible gene expression during late third-instar developmental stages can explain the potential impairment of metamorphosis induction seen upon ubiquitous or PG-specific *Nup107* knockdown. In addition to the reduced size of the salivary gland and brain complex, we also noticed a compromise in the size of the Prothoracic gland upon *Nup107* knockdown (Figure S7).

These observations suggest that Nup107 exerts a regulation on ecdysone biosynthesis and active 20E-EcR complex formation rather than playing a direct role in EcR nuclear translocation.

Nup107 **exerts control on the EcR pathway through Ecdysone level regulation**

We reasoned that Nup107 may regulate the ecdysone biosynthesis in PG to induce the larval stage growth arrest. We delved into analyzing the effect of *Nup107* knockdown on ecdysone production. The considerable decrease in PG size due to *Nup107* knockdown (Figure S7) can potentially reduce 20E production. This prompted us to explore the potential role of Nup107 in influencing ecdysone production, and we assessed the impact of *Nup107* knockdown on ecdysone biosynthesis.

Utilizing an ELISA-based detection method, we assessed 20E levels in larvae at 96 hours and 120 hours after egg laying (AEL). Larvae from different experimental conditions, including control, ubiquitous *Nup107*-depletion, and PG-specific *Nup107*-depletion, were used in this analysis. Strikingly, the results indicated a substantial decrease (~ 3-fold with ubiquitous and ~10-fold for PG-specific knockdown) in total 20E

levels upon *Nup107* knockdown, particularly at 120 AEL which coincides with the 20E surge seen during metamorphosis (Figures 4A and S8A). This observation is crucial and suggests a potential defect in ecdysone biosynthesis in *Nup107*-depleted organisms.

As depicted in Figure 4B, the PTTH hormone signaling in the PG upregulates the expression of *Halloween* genes (*spookier*, *phantom*, *disembodied*, and *shadow*) responsible for ecdysone biosynthesis, and the *shade* gene product is required for active 20E generation in peripheral tissues (Christensen et al., 2020; McBrayer et al., 2007; Shimell et al., 2018). We analyzed the *Halloween* genes transcript level in *Nup107*-depleted larvae and observed a significant downregulation for each of the *Halloween* quartet genes mentioned earlier. (Figures 4C-4F and S8B-S8E). Further, the level of the *shade* gene required for converting precursor ecdysone to active 20E was also reduced twofold in *Nup107*-depleted larvae (Figures 4G and S8F).

20E rescues Nup107-dependent EcR localization defects

The observed correlation between the expression levels of ecdysone biosynthetic genes and reduced levels of 20E upon *Nup107* knockdown strongly suggests a role for Nup107 in 20E biosynthesis, active 20E-EcR complex formation, and its nuclear translocation. It is not surprising in this context that exogenous ecdysone supplementation through larval food rescues pupariation blocks arising from ecdysone deficiency (Garen et al., 1977; Ou et al., 2016; Shimell et al., 2018). We experimented the same under *Nup107*-depletion conditions and supplemented exogenous ecdysone to PG-specific *Nup107*-depleted larvae by feeding them with a diet enriched with 20-hydroxyecdysone (0.2 mg/ml). Supplementation of 20E to *Nup107*-depleted larvae significantly (70-80%) alleviated the developmental arrest, and the onset of pupariation was comparable to the control (Table S1). However, none of the pupae could eventually eclose successfully, probably due to other effects of *Nup107* depletion. We asked if nuclear translocation of EcR can also be rescued by exogenous supplementation of 20E. While incubation of salivary glands of late third instar larva in S2 media control alone did not rescue EcR localization in any of the *Nup107*-knockdown genotypes (Figures 5A-5C and S9A), we noticed a complete EcR nuclear translocation rescue in

ubiquitous as well as PG-specific *Nup107*-depleted salivary glands when incubated with 20E (Figures 5D-5F and S9B).

The exogenous supplementation of 20E leads to active 20E-EcR complex formation as mRNA levels of the *Eip75A* and *Eip74EF* target genes were rescued significantly back to normal levels (Figures 5G and 5H). Overall, these findings highlight the important regulatory function of Nup107 in the ecdysone signaling pathway.

***Torso* is an effector of *Nup107* mediated functions in metamorphosis**

Next, we explored the mechanism of Nup107-driven regulation of 20E levels and metamorphosis. Receptor tyrosine kinase family of cell surface receptors signal by binding to ligands (growth factors and hormones) and participate in metabolism, cell growth, and development. Among these RTKs, the Torso, belonging to the platelet-derived growth factor receptor (PDGFR) class, plays a significant role during metamorphosis by serving as a receptor for the neuropeptide PTTH in the *Drosophila* brain (Sopko & Perrimon, 2013).

Functional engagement of PTTH-Torso activates the MAP kinase pathway, involving components of Ras, Raf, MEK, and extracellular signal-regulated kinase (ERK), thereby initiating metamorphosis (Figure 6A). The *torso* knockdown in the prothoracic glands resulted in the developmental arrest phenotype synonymous with what is observed with *Nup107* knockdown. Feeding 20E to *torso*-depleted larvae completely rescued developmental delay and normal growth phenotypes (Rewitz et al., 2009). We observed a significant decrease in the *torso* levels (~ four-fold) when *Nup107* was depleted ubiquitously using *Actin5C-GAL4* (Figure 6B), suggesting an epistatic regulation by Nup107 on the torso. Further, the phenotypic similarity between *Nup107* and *torso*-depletion scenarios and diminished *torso* level upon *Nup107*-depletion prompted us to investigate whether the *torso* is an effector of Nup107.

Overexpression of the *torso* and or ras^{V12} have been utilized to rescue torso pathway-mediated defects (Cruz et al., 2020; Rewitz et al., 2009). We probed the possibility of *Nup107* phenotype rescue by ubiquitous or PG-specific overexpression of the *torso* and ras^{V12}. Overexpression of either *torso* or ras^{V12} in *Nup107*-depletion background

completely rescued the pupariation defects (Figures 6C and 6D). The *torso* overexpression-mediated rescue of Nup107-depletion phenotypes is specific as overexpression of *Egfr* (another RTK implicated in metamorphosis) and *Usp* (co-receptor with EcR) in *Nup107* depletion background could not rescue the pupariation defects (data not shown). The remarkable rescue demonstrated by *torso* overexpression prompted us to analyze the status of EcR nuclear translocation, ecdysone biosynthesis, and ecdysone-inducible gene expression. The restoration of EcR nuclear translocation (Figures 6E-6G), the ecdysone biosynthesis genes, *spookier*, *phantom*, *disembodied*, and *shadow* (Figures S10B-S10E), and ecdysone target genes *Eip75A* and *Eip74EF* (Figures 6H and 6I) to control levels indicated that *torso* could efficiently rescue *Nup107* phenotypes.

These observations suggest that the *torso* is a downstream effector of Nup107 functions, and torso-dependent signaling, responsible for 20E synthesis in PG and metamorphosis, is regulated by Nup107 levels.

Discussion

Apart from its importance in mRNA export and cell division at the cellular level, the NPCs Y-complex member Nup107, when mutated, correlates with developmental abnormalities, microcephaly, and nephrotic syndrome (Miyake et al., 2015; Zheng et al., 2012). In several human cancer types, Nup107 exhibits high expression and serves as a biomarker for hepatocellular carcinoma. A strong structural and functional conservation between human and *Drosophila* Nup107 proteins allows *Drosophila* to be used to model to gain mechanistic insights in Nup107 functions in human diseases (Shore et al., 2022; Weinberg-Shukron et al., 2015). We observe that Nup107 is involved in critical developmental transitions from larva to pupa during *Drosophila* development as pupariation is completely arrested (Figure 1). The foraging third instar larva must acquire a critical weight and sufficient energy stores before it can metamorphose into a non-feeding pupa, molting into a healthy adult. The activation of the Torso receptor and sequent surge in ecdysone synthesis is essential for larval to

pupal transition (Christensen et al., 2020; Hao et al., 2021; Luo et al., 2024). The elevated ecdysone levels trigger the translocation of the heterodimeric ecdysone receptor [in complex with Ultraspiracle (Usp)] into the nucleus to induce pupariation-specific transcriptional programming (Johnston et al., 2011). Similarly, when *Nup107* is depleted, nuclear translocation of EcR is abolished, arresting metamorphosis at the level of the third instar larval stage (Figure 2).

Translocation of nuclear receptor proteins like the ecdysone receptor to the nucleus is a crucial step for transcriptional activation. Nup358, present at the cytoplasmic filament face of NPC, plays a vital role in the nuclear import of Met (juvenile hormone receptor) along with Hsp83 (He et al., 2017) to help maintain the larval stages of development. The marked absence of EcR from the nucleus was intriguing as Nup107 generally participates in the nuclear export process. Perhaps Nup107 regulates pupariation by modulating ecdysone synthesis, ecdysone signaling, and nuclear translocation of EcR. Surprisingly, Nup107 is dispensable for the nuclear translocation of EcR in the target tissue, the salivary gland cells (Figure 3). Nup107 exerts strong control over the expression of *Halloween* genes involved in ecdysone biosynthesis, resulting in diminished 20E titer, poor EcR activation, and delayed larva-to-pupa transition (Figures 4 and S6). The effect of Nup107 on *Halloween* genes adheres well with pupariation defects. These observations are in concurrence with reports of low ecdysone levels disrupting the pupariation process, leading to a halt in insect development (Christensen et al., 2020; Cruz et al., 2020).

In addition to ecdysone signaling, insect metamorphosis also has a strong contribution from receptor tyrosine kinase RTK pathway signaling. Notably, Torso signaling is essential for embryonic development and metamorphosis in *Drosophila*. The receptor expression level impacts the signaling output: high receptor levels trigger a robust and transient signal, while lower levels result in a weaker, sustained signal (Jenni et al., 2015; Konogami et al., 2016). Accordingly, the reduced ecdysone levels in the *torso* knockdown prothoracic glands induced pupariation delays (Rewitz et al., 2009). We observe a similar defect with *Nup107* knockdown, indicating a possible reduction in *torso* levels. Interestingly, we observed significantly reduced torso levels in *Nup107*-

depleted organisms, suggesting an essential upstream function for Nup107 in regulating RTK pathway activation and the associated *Drosophila* metamorphosis process. In the contrasting observation, *Nup107* depleted larval tissues (salivary glands, brain complex, and prothoracic gland) are significantly smaller in size (Figures S3 and S7). It is important to know how Nup107 contributes to organ size maintenance and if a crosstalk with RTK signaling is required in this context.

The developmental delays observed in *Nup107* knockdown larvae can be restored by exogenous supplementation of 20E, suggesting that Nup107 can modulate directly or indirectly the Torso receptor activity for ecdysone production and developmental regulation. Accordingly, we successfully rescued developmental delays by ubiquitous and PG-specific *torso* overexpression. Perhaps overexpression of the torso pathway mediator molecules can rescue the *Nup107* developmental delay phenotypes. The oncogenic variant of the Ras-GTPase (ras^{V12}) has been explored in a similar analysis with torso pathway mutants (Cruz et al., 2020; Rewitz et al., 2009). The alleviation of the developmental delays in the *Nup107* knockdown background upon ras^{V12} overexpression is an indication of Nup107 serving as an epistatic regulator of the torso pathway in metamorphic transitions (Figure 6).

In essence, our findings indicate that Nup107 influences pupariation timing by regulating the torso levels, it's signaling, and ecdysone biosynthesis (Figure 7). Previous research has shown that nuclear pore complexes (NPCs) are essential for maintaining global genome organization and regulating gene expression (Capelson, Doucet, et al., 2010; Capelson, Liang, et al., 2010; Iglesias et al., 2020). Particularly, Nup107 interacts with chromatin and targets active gene domains to regulate gene expression (Gozalo et al., 2020). Thus, Nup107 exerting its effects on *torso* transcription is the primary regulatory event in the *Drosophila* metamorphosis. It is important to note that the synthesis and availability of Torso ligand, PTTH, may not be affected by the Nup107 since torso or downstream effector ras^{V12} overexpression is sufficient to rescue the developmental arrest phenotype. It is thus crucial to further delineate the mechanism of Nup107-dependent regulation on *torso* pathway activation. The whole genome transcriptomics from PG can help shed more light on the regulatory roles of Nup107. This information

will offer valuable insights into how nucleoporins regulate gene expression and serve as a model for elucidating how they govern the temporal specificity of developmental processes in organisms. These analyses will help establish a link between Nup107, the PTTH-PG axis, and the regulation of maturation timing. Our observations indicate critical roles for Nup107 in both torso-ecdysone interplay in metamorphosis and torso-independent mechanism for organ size maintenance. Together they add valuable information to hitherto unknown functions of the Nup107 in organismal development. Further investigations are required to identify the interactors of Nup107 involved in these coordination mechanisms in developmental transition.

Materials and methods

Key resources table

Reagent type (species) or resource	Designation	Source or reference	Identifiers	Additional information
Genetic reagent (*D. melanogaster*)	w^{1118}	Bloomington *Drosophila* Stock Center	BDSC:3605; FLYB: FBst000360; RRID:BDSC_3605	w[1,118]
Genetic reagent (*D. melanogaster*)	w1118; P{GD12024} v22407	Vienna *Drosophila* Resource Center	VDRC: v22407; FLYB: FBst0454535; RRID:FlyBase_FBst0454535	P{GD12024}v22407 ($Nup107^{GD}$ RNAi)
Genetic reagent (*D. melanogaster*)	P{KK108047 }VIE-260B	Vienna *Drosophila* Resource Center	VDRC: v110759; FLYB: FBst0482324; RRID:FlyBase_FBst0482324	P{KK108047}VIE-260B ($Nup107^{KK}$ RNAi)
Genetic reagent (*D. melanogaster*)	y[1] w[*]; P{w[+mW.hs]=GawB}AB1	Bloomington *Drosophila* Stock Center	BDSC:1824; FLYB: FBti0001249; RRID:BDSC_1824	AB1-Gal4
Genetic	y[1] w[*];	Bloomington	BDSC:80577;	Phm-Gal4

reagent (*D. melanogaster*)	P{w[+mC]=phtm-GAL4.O}22	*Drosophila* Stock Center	FLYB: FBti0201787; RRID:BDSC_80577	
Genetic reagent (*D. melanogaster*)	y[1] w[*]; P{Act5C-GAL4-w}E1/CyO	Bloomington *Drosophila* Stock Center	BDSC:25374; FLYB: FBti0127834; RRID:BDSC_25374	Actin5C-Gal4
Genetic reagent (*D. melanogaster*)	w[*]; wg[Sp-1]/CyO; P{w[+mC]=mRFP-Nup107.K}7.1	Bloomington *Drosophila* Stock Center	BDSC:35517; FLYB: FBti0130064; RRID:BDSC_35517	mRFP-Nup107
Genetic reagent (*D. melanogaster*)	y[1] M{w[+mC]=nanos-Cas9.P}ZH-2A w[*]	Bloomington *Drosophila* Stock Center	BDSC:54591; FLYB: FBti0159183; RRID:BDSC_54591	Nanos.Cas9
Genetic reagent (*D. melanogaster*)	w[*]; TI{w[+mW.hs]=TI}trk[Delta]/CyO; P{w[+mC]=UASp-tor.G}5.7	Bloomington *Drosophila* Stock Center	BDSC:92604; FLYB: FBti0216047; RRID:BDSC_92604	UAS-torso
Genetic reagent (*D. melanogaster*)	w[1118]; P{w[+mC]=UAS-Ras85D.V12}TL1	Bloomington *Drosophila* Stock Center	BDSC:4847; FLYB: FBti0012505; RRID:BDSC_4847	UAS-ras^{V12}
Genetic reagent (*D. melanogaster*)	Nup107^{KK};UAS-GFP	This paper	N/A	
Genetic reagent (*D. melanogaster*)	*UAS-GFP;Nup107^{GD}*	This paper	N/A	
Genetic reagent (*D. melanogaster*)	*UAS-GFP;Phm-Gal4/TM6.Tb*	This paper	N/A	
Genetic reagent (*D. melanogaster*)	*Nup107 gRNA line*	This paper	N/A	
Genetic reagent (*D. melanogaster*)	*Nup107KK;UAS-torso*	This paper	N/A	
Genetic reagent (*D. melanogaster*)	*Nup107KK;UAS-rasV12*	This paper	N/A	

Antibody	Anti-Nup107 (Rabbit polyclonal)	This paper	N/A	WB (1:500) IF (1:100)
Antibody	Anti- Nuclear Pore Complex Proteins (Mouse monoclonal)	Biolegend	Cat#902902 (MAb414)	IF (1:500)
Antibody	Anti-EcR (Mouse monoclonal)	DSHB	Cat#DDA2.7	IF (1:20)
Antibody	Anti-α tubulin (Mouse monoclonal)	DSHB	Cat#12G10	IB (1:5000)
Antibody	Goat anti-rabbit Alexa-Fluor Plus 680	Thermo Fisher Scientific	Cat#A32734	IB (1:40000)
Antibody	Goat anti-mouse Alexa-Fluor Plus 800	Thermo Fisher Scientific	Cat#A32730	IB (1:40000)
Antibody	Goat anti-rabbit Alexa Fluor 488	Thermo Fisher Scientific	Cat#A11034	IF (1:800)
Antibody	Goat anti-rabbit Alexa Fluor 568	Thermo Fisher Scientific	Cat#A11036	IF (1:800)
Antibody	Goat anti-mouse Alexa Fluor 488	Thermo Fisher Scientific	Cat#A11029	IF (1:800)
Antibody	Goat anti-mouse Alexa Fluor 568	Thermo Fisher Scientific	Cat#A11004	IF (1:800)
Antibody	Goat anti-rabbit Alexa Fluor 647	Jackson Immuno Research	Cat#111-605-045	IF (1:800)
Sequence-based reagent	Nup107_gRNA1	This paper	PCR primers (5'–3'):	TGGCCGACAGCCCGTTCCCG
Sequence-based reagent	Nup107_gRNA2	This paper	PCR primers (5'–3'):	GGAGCTGCTCAACTCGAAACTGG
Sequence-based reagent	5’UTR Primer1_F	This paper	PCR primers (5'–3'):	GCTCCCAAATACTCGCTGCC
Sequence-	3’UTR	This paper	PCR primers	CTTCTGCCGGCGGATTTG

based reagent	Primer1_R		(5'–3'):	TT
Sequence-based reagent	5'UTR Primer2_F	This paper	PCR primers (5'–3'):	GGTACCCCATACTAATGATTC
Sequence-based reagent	3'UTR Primer2_R	This paper	PCR primers (5'–3'):	CATGTTGTTTGTCTCGCTACT
Sequence-based reagent	Nup107 (for antibody generation)	This paper	PCR primers (5'–3'):	Forward: ATCGGATCCATGGCCGACAGCCCGTTC Reverse: ATCGAATTCCTACCACGCCATCATACGATC
Sequence-based reagent	Nup107_RT	This paper	PCR primers (5'–3'):	Forward: GCAGGCTCACCGATCGGAAG Reverse: TCCATCTGCAGTAGGCGATG
Sequence-based reagent	EcR_RT	This paper	PCR primers (5'–3'):	Forward: AAGAGGATCTCAGGCGTATAA Reverse: GGCCTTTAGTAACGTGATCTG
Sequence-based reagent	Eip75A_RT	This paper	PCR primers (5'–3'):	Forward: ACCACAGCACCACCCATTT Reverse: TGTTTGGCGGTAGTTTCAGG
Sequence-based reagent	Eip74EF_RT	This paper	PCR primers (5'–3'):	Forward: CTCTGCTCCACATAAAGACG Reverse: CCGCTAAGCAGATTGTGG
Sequence-based reagent	Phm_RT	This paper	PCR primers (5'–3'):	Forward: GGATTTCTTTCGGCGCGATGTG Reverse: TGCCTCAGTATCGAAAAGCCGT
Sequence-based reagent	Spok_RT	This paper	PCR primers (5'–3'):	Forward: TATCTCTTGGGCACACTCGCTG Reverse: GCCGAGCTAAATTTCTCCGCTT
Sequence-based	Dib_RT	This paper	PCR primers (5'–3'):	Forward: TGCCCTCAATCCCTATCTG

reagent				GTC Reverse: ACAGGGTCTTCACACCCATCTC
Sequence-based reagent	Sad_RT	This paper	PCR primers (5'–3'):	Forward: CCGCATTCAGCAGTCAGTGG Reverse: ACCTGCCGTGTACAAGGAGAG
Sequence-based reagent	Shd_RT	This paper	PCR primers (5'–3'):	Forward: CGGGCTACTCGCTTAATGCAG Reverse: AGCAGCACCACCTCCATTTC
Sequence-based reagent	Torso_RT	This paper	PCR primers (5'–3'):	Forward: CAGCTACTGCGACAAGGTCATCG Reverse: CTCGGTTGCAGCTTGCAGTTG
Sequence-based reagent	Rpl49_RT	This paper	PCR primers (5'–3'):	Forward: CGTTTACTGCGGCGAGAT Reverse: GTGTATTCCGACCACGTTACA
Commercial assay or kit	RNA isolation kit	Favorgen Biotech	Cat#FATRK-001-2	
Commercial assay or kit	iScriptTM cDNA synthesis kit	BIORAD	Cat#170-8891	
Commercial assay or kit	20-hydroxyecdysone ELISA kit	Thermo Fisher Scientific	Cat#EIAHYD	
Chemical compound, drug	Fluoroshield	Sigma-Aldrich	Cat#F6057	
Chemical compound, drug	TritonX-100	Sigma-Aldrich	Cat#X100-1L	
Chemical compound, drug	Tween-20	Sigma-Aldrich	Cat#274348	
Chemical compound, drug	Paraformaldehyde	Sigma-Aldrich	Cat#158127	

Chemical compound, drug	iTaq Universal SYBR® Green Supermix	BIORAD	Cat#1725122	
Chemical compound, drug	G9 Taq Polymerase 10X buffer with MgCl2	GCC Biotech	Cat#G7115	
Chemical compound, drug	dNTPs	SBS GENETECH	Cat#EN-2	
Chemical compound, drug	20-hydroxyecdysone	Sigma-Aldrich	Cat# H5142	
Chemical compound, drug	EDTA	Sigma-Aldrich	Cat#03690	
Chemical compound, drug	SDS	HIMEDIA	Cat#GRM886	
Chemical compound, drug	Proteinase-K	MP Biomedicals	Cat#193981	
Chemical compound, drug	Tris	HIMEDIA	Cat#MB029	
Chemical compound, drug	Potassium acetate	HIMEDIA	Cat#MB042	
Chemical compound, drug	Isopropanol	MP Biomedicals	Cat#194006	
Chemical compound, drug	Ethanol	Merck	Cat#100983	
Chemical compound, drug	Sucrose	ANJ Biomedicals	Cat#100314	
Chemical compound, drug	IPTG	Sigma-Aldrich	Cat#I6758	
Chemical compound, drug	Protease inhibitor Cocktail (PIC)	Roche	Cat#04693132001	
Chemical compound, drug	NaCl	Emparta ACS	Cat#1.93206.0521	
Chemical	EGTA	Sigma-	Cat#E4378	

compound, drug		Aldrich		
Chemical compound, drug	Sodium deoxycholate	Sigma-Aldrich	Cat# 30970	
Chemical compound, drug	Sodium azide	Sigma-Aldrich	Cat#438456	
Chemical compound, drug	N-Hydroxy-succinimidyl (NHS) Sepharose	Sigma-Aldrich	Cat#H8280	
Chemical compound, drug	Urea	MP Biomedicals	Cat#194857	
Software, algorithm	ImageJ/FIJI	National Institutes of Health, USA		http://imagej.nih.gov/ij/
Software, algorithm	GraphPad Prism Software	GraphPad		https://www.graphpad.com/
Software, algorithm	Adobe Photoshop 2023	Adobe		https://www.adobe.com/in/products/photoshop.html
Software, algorithm	QuantStudio Design & Analysis Software	Applied Biosystems		https://www.thermofisher.com/in/en/home/technical-resources/software-downloads/quantstudio-3-5-real-time-pcr-systems.html

Fly stocks and genetics

Experimental *Drosophila melanogaster* stocks were reared on a standard cornmeal diet (Nutri-Fly Bloomington formulation) under controlled conditions of 25°C and 60% relative humidity unless otherwise specified. Fly lines used in this study were sourced from the Bloomington *Drosophila* Stock Centre (BDSC) at Indiana University or from the Vienna *Drosophila* Resource Center (VDRC), which are listed in the Key resources table. The UAS-GFP lines were received as a gift from Dr. Varun Chaudhary (IISER Bhopal, India). Control groups were generated through crosses between the driver line and w^{1118} flies. For RNA interference (RNAi) experiments, crosses were maintained at 29°C to optimize GAL4 expression. The $Nup107^{GD}$ line, in conjunction with *Actin5C-*

GAL4, was specifically cultivated at 23°C to generate third-instar larvae for experimental purposes.

Transgenic fly generation

In the generation of transgenic flies containing gRNA, we employed a systematic approach. The online tool available at http://targetfinder.flycrispr.neuro.brown.edu was used for the initial sgRNA design, ensuring zero predicted off-targets. Subsequently, we utilized an additional tool available at https://www.flyrnai.org/evaluateCrispr/ to evaluate and score the predicted efficiency of sgRNAs in the targeted region. The most efficient sgRNAs, demonstrating high specificity with no predicted off-targets, were selected and cloned into the pCFD4 vector. The Fly Facility services at the Centre for Cellular and Molecular Platforms, National Center for Biological Sciences (C-CAMP-NCBS), Bangalore, India, were utilized to clone and generate transgenic flies. Primer sequences employed in this study can be found in the Key resources table.

CRISPR –Cas9 mediated mutant Generation

Virgin nanos.Cas9 (BL-54591) flies were crossed with males of gRNA transgenic lines, and approximately 10 F1 progeny males were crossed with balancer flies specific for the gene of interest. A single-line cross was established using the F2 progeny to assess the deletion of *nup107*. Subsequently, F3 progeny were subjected to nested PCR to confirm deletions. Positive individuals were further tested for the presence of gRNA and Cas9 transgenes, and flies lacking both were propagated into stocks.

Genomic DNA Isolation

Approximately ten flies were homogenized in 250 µL of solution A, comprising 0.1 M Tris-HCl, pH 9.0, 0.1 M EDTA, and 1% SDS, supplemented with Proteinase-K. The homogenate was incubated at 70°C for 30 min. Subsequently, 35 µL of 8 M potassium acetate was added, mixed gently without vortexing, and incubated on ice for 30 min. The homogenate was then centrifuged at 13,000 rpm at 4°C for 15 min, and the supernatant was carefully collected without disturbing precipitates or the interphase. 150 µL of Isopropanol was added to the supernatant and incubated on ice for 15 min. After centrifugation at 13,000 rpm for 5 min, the supernatant was discarded, and the

pellet was washed with 1 mL of 70% ethanol by centrifuging at 13,000 rpm for 5 min. The supernatant was again discarded, and the pellet was dried at 55°C until the ethanol evaporated. Finally, the pellet was resuspended in 50 µL of Tris-EDTA buffer and incubated at 37°C.

Nested PCR

Nested PCR was employed to assess the presence of deletions in flies, utilizing genomic DNA as the template. 1 µL of DNA was used for the initial PCR with an outer set of primers (Key resources table). Following this, 1 µL of the initial PCR product was employed for a subsequent PCR with an inner set of primers. The resulting PCR products were then resolved on 0.8% agarose gel to visualize the desired bands indicative of deletions.

Measurement of developmental timing and pupariation

Flies were permitted to lay eggs for 3 hours on agar plates supplemented with yeast, synchronizing the larvae. Newly hatched L1 larvae were then collected and transferred to vials. Pupariation times and dates were recorded daily during the light cycle. Data from 8-10 vials were aggregated, organized by pupariation time and cumulative percentage pupariation, and analyzed using Microsoft Excel.

Antibody generation and western blotting

To generate antibodies against *Drosophila Nup107* (CG6743), the N-terminal 210 amino acids, recognized as the most unique and antigenic region, were sub-cloned into the modified tag-less pET28a(+) vector, pET28a(+)-JK vector. The protein was expressed in *Escherichia coli* BL21 (DE3) cells, induced with 200 µM IPTG (Sigma), and incubated at 30°C for 4 hours. Following cell pelleting, the pellet was resuspended in lysis buffer (50 mM Tris pH 8.0, 1 mM EDTA, and 25% Sucrose) with 1× protease inhibitor mixture (Roche Applied Science), and lysozyme (from 50 mg/mL stock) was added to facilitate bacterial lysis. After sonication and centrifugation, the pellet was successively resuspended in inclusion body buffer I (20 mM Tris pH 8.0, 0.2 M NaCl, 1% Sodium deoxycholate, and 2 mM EGTA) and buffer II (10 mM Tris pH 8.0, 0.25% Sodium deoxycholate and 1 mM EGTA) and centrifuged. This process was repeated

three times within inclusion body buffer II, and the final pellet was dissolved in 8 M Urea buffer (10 mM Tris-HCl pH 8.0, 8 M Urea, 0.1 mM NaN_3, and 1 mM EGTA), diluted to 6 M Urea, and centrifuged. The supernatant was loaded onto SDS-PAGE, and the desired band was cut for protein elution. Rabbit polyclonal antibodies against Nup107 were generated at Bio Bharati Life Sciences Pvt. Ltd., Kolkata, West Bengal, India. The antibodies obtained were subjected to affinity purification. The purification involved the chemical cross-linking of purified antigens to N-hydroxy succinimidyl-Sepharose beads (Sigma). The elution process was carried out under low pH conditions, followed by neutralization. Subsequently, the eluted antibodies were dialyzed against phosphate-buffered saline (PBS) overnight at 4°C to remove any remaining impurities and optimize their stability and functionality for subsequent experimental use.

Larval brain complexes from third-instar larvae were dissected, lysed in Laemmli buffer, and resolved on 8% SDS-PAGE. Two equivalent head complexes were loaded per well. After transfer to a polyvinylidene difluoride membrane, blocking was performed with 5% fat-free milk. The membrane was then incubated with polyclonal anti-Nup107 antibody (1:500) and anti-α-tubulin (DSHB, 12G10) (1:5000) at 4°C overnight. Following three washes with TBS-T buffer (20 mM Tris-HCl pH 7.5, 150 mM NaCl, 0.1% Tween-20), the membrane was incubated with secondary antibodies, anti-rabbit-Alexa-Fluor Plus 680 (Thermo Fisher Scientific #A32734) and anti-mouse-Alexa-Fluor Plus 800 (Thermo Fisher Scientific #A32730). Following incubation with secondary antibodies, the membrane was washed three times for 10 minutes each with Tris-buffered saline containing Tween-20 (TBS-T) to remove unbound antibodies. The washed membrane was then subjected to imaging using the Li-Cor IR system (Model: 9120), allowing for the visualization and analysis of the protein bands on the membrane.

Immunostaining

For immunostaining *Drosophila* salivary glands, the previously reported protocol was followed (Mehta et al., 2021). The larvae were dissected in cold phosphate-buffered saline (PBS) to isolate salivary glands. Glands underwent pre-extraction with 1% PBST (PBS + 1% Triton X-100), then fixation in freshly prepared 4% paraformaldehyde for 30 minutes at room temperature. Subsequently, the glands were thoroughly washed with

0.3% PBST (0.3% Triton X-100 containing PBS). Blocking was performed for 1 h with 5% normal goat serum (#005-000-001, The Jackson Laboratory, USA). The glands were stained with the following primary antibodies: anti-Nup107 (1:100), mAb414 (1:500, Bio-legend) and anti-EcR (1:20, DDA2.7, DSHB) overnight at 4°C. Tissues were washed three times with 0.3% PBST (PBS + 0.3% Triton X-100), followed by incubation with secondary antibodies: anti-rabbit Alexa Fluor 488 (1:800, #A11034, Thermo Fisher Scientific), anti-rabbit Alexa Fluor 568 (1:800, #A11036, Thermo Fisher Scientific), anti-mouse Alexa Fluor 488 (1:800, #A11029, Thermo Fisher Scientific), anti-mouse Alexa Fluor 568 (1:800, #A11004, Thermo Fisher Scientific), and anti-rabbit Alexa Fluor 647 (1:800, Jackson ImmunoResearch). Following secondary antibody incubation, tissues were washed three times with 0.3% PBST (PBS + 0.2% Triton X-100) and mounted with DAPI-containing Fluoroshield (#F6057, Sigma). The same protocol was followed for staining of the Brain complex and prothoracic gland.

Fluorescence Intensity quantification

Images were acquired using an Olympus Confocal Laser Scanning Microscope FV3000. Subsequent image processing was conducted using the Fiji software, and signal intensities were averaged using GraphPad software (Prism). To quantify the EcR nuclear to cytoplasmic ratio, three distinct regions of interest (ROI) were designated per nucleus and its surrounding cytoplasm. Fiji software measured the average intensity in each ROI, and the mean of these intensities was determined per nucleus and its adjacent cytoplasm. The final graph depicts the ratio of the mean intensities observed in the nucleus to that in the cytoplasm. All experiments were conducted with a minimum of three independent replicates.

Quantitative RT-PCR

Total RNA was extracted from various genotypes (control, ubiquitously depleted *Nup107*, and prothoracic gland-specific depletion of *Nup107*) of whole late third instar larvae utilizing the total tissue RNA isolation kit (Favorgen Biotech). One microgram of total RNA was employed for cDNA synthesis with the iScript cDNA synthesis kit (Bio-Rad). The resulting cDNA was diluted fivefold, and 1 µL from each genotype was utilized as a template. RT-PCR was conducted using SYBR Green PCR master mix on

an Applied Biosystems QuantStudio 3 Real-Time PCR System. The Rpl69 gene served as the control, and relative transcript levels were determined using the CT value ($2^{-\Delta\Delta CT}$). Differences in gene expression were analyzed using Student's t-test, with a p-value < 0.05 considered significant. The primers used are detailed in the Key resources table. The resultant graph illustrated the fold change in gene expression, plotted using GraphPad software (Prism).

20-hydroxyecdysone (20E) level measurements

Three biological replicates of 25 mg larvae from each genotype were collected at the specified times after egg laying (AEL). The larvae were washed, dried, and weighed before being flash-frozen on dry ice and stored at -80°C. Ecdysone extraction was done by thoroughly homogenizing the frozen samples in 300 µL ice-cold methanol with a plastic pestle. After centrifugation at 17,000 x g for 10 minutes, the supernatant was divided into two Eppendorf tubes containing approximately 150 µL supernatant. Methanol from both tubes was evaporated in a vacuum centrifuge for 60 minutes, and the resulting pellets were redissolved by adding 200 µL Enzyme Immunoassay (EIA) buffer to one of the tubes. After vortexing, the same 200 µL EIA buffer was transferred to the second tube, followed by another round of vortexing. The Enzyme-Linked Immunosorbent Assay (ELISA) was performed using a 20-hydroxyecdysone ELISA kit (#EIAHYD) from Thermo Fisher Scientific.

20E Rescue Experiment

20-hydroxyecdysone (#H5142, Sigma) was dissolved in ethanol to achieve a 5 mg/mL concentration. Salivary glands from third instar larvae of different genotypes were extracted and then incubated for 6 hours in Schneider's S2 media with 50 µM 20E. After the incubation, the glands underwent procedures for immunostaining and RNA extraction.

To facilitate the rescue of the larvae through feeding, 30-third instar larvae, *Nup107* depleted larvae cultured at 29°C incubator, were first washed with water. They were then transferred to vials containing either 20E (at a final concentration of 0.2 mg/mL) or 95% ethanol (in the same amount as the 20E). Once the larvae were added to the vials,

these were returned to the 29°C incubator and observed for pupariation, recording the time of this developmental stage.

Competing interests

The authors declare no competing interests.

Acknowledgments

We thank the Bloomington *Drosophila* Stock Centre (BDSC) and Vienna *Drosophila* Resource Centre (VDRC) for generously providing the fly lines crucial for this study. Special recognition is given to Bio Bharati Life Sciences Pvt. Ltd., Kolkata, India, for their significant contribution to antibody generation and the Developmental Studies Hybridoma Bank (DSHB) for supplying antibodies. Our sincere thanks go to C-CAMP Bengaluru for their instrumental role in generating the transgenic fly. BioRender was used to create models wherever necessary. The Indian Institute of Science Education and Research Bhopal Central Instrumentation Facility is acknowledged for its valuable support in DNA sequencing and facilitating access to confocal microscopes. This work is supported by the Science and Engineering Research Board grant no. CRG/2020/000496 provided to RKM.

Author Contribution

JK and RKM conceptualized the project and the experimental plan and wrote the manuscript. JK performed all experiments and analyzed data. PAJ made initial observations with Nup107 RNAi and analyzed and discussed data. RKM provided intellectual support in data analysis and secured funding for the project.

Data and Resource Availability

All relevant data and resource can be found within the article and its supplementary information.

References

Bai, S. W., Rouquette, J., Umeda, M., Faigle, W., Loew, D., Sazer, S., & Doye, V. (2004). The fission yeast Nup107-120 complex functionally interacts with the small GTPase Ran/Spi1 and is required for mRNA export, nuclear pore distribution, and proper cell division. *Mol Cell Biol*, *24*, 6379-6392. https://doi.org/10.1128/MCB.24.14.6379-6392.2004

Boehmer, T., Enninga, J., Dales, S., Blobel, G., & Zhong, H. (2003). Depletion of a single nucleoporin, Nup107, prevents the assembly of a subset of nucleoporins into the nuclear pore complex. *Proc Natl Acad Sci U S A*, *100*, 981-985. https://doi.org/10.1073/pnas.252749899

Capelson, M., Doucet, C., & Hetzer, M. W. (2010). Nuclear pore complexes: guardians of the nuclear genome. *Cold Spring Harb Symp Quant Biol*, *75*, 585-597. https://doi.org/10.1101/sqb.2010.75.059

Capelson, M., Liang, Y., Schulte, R., Mair, W., Wagner, U., & Hetzer, M. W. (2010). Chromatin-bound nuclear pore components regulate gene expression in higher eukaryotes. *Cell*, *140*, 372-383. https://doi.org/10.1016/j.cell.2009.12.054

Christensen, C. F., Koyama, T., Nagy, S., Danielsen, E. T., Texada, M. J., Halberg, K. A., & Rewitz, K. (2020). Ecdysone-dependent feedback regulation of prothoracicotropic hormone controls the timing of developmental maturation. *Development*, *147*. https://doi.org/10.1242/dev.188110

Cronauer, M. V., Braun, S., Tremmel, C., Kroncke, K. D., & Spindler-Barth, M. (2007). Nuclear localization and DNA binding of ecdysone receptor and ultraspiracle. *Arch Insect Biochem Physiol*, *65*, 125-133. https://doi.org/10.1002/arch.20184

Cronshaw, J. M., Krutchinsky, A. N., Zhang, W., Chait, B. T., & Matunis, M. J. (2002). Proteomic analysis of the mammalian nuclear pore complex. *J Cell Biol*, *158*, 915-927. https://doi.org/10.1083/jcb.200206106

Cruz, J., Martin, D., & Franch-Marro, X. (2020). Egfr Signaling Is a Major Regulator of Ecdysone Biosynthesis in the Drosophila Prothoracic Gland. *Curr Biol*, *30*, 1547-1554 e1544. https://doi.org/10.1016/j.cub.2020.01.092

D'Angelo, M. A., & Hetzer, M. W. (2008). Structure, dynamics and function of nuclear pore complexes. *Trends Cell Biol*, *18*, 456-466. https://doi.org/10.1016/j.tcb.2008.07.009

Garen, A., Kauvar, L., & Lepesant, J. A. (1977). Roles of ecdysone in Drosophila development. *Proc Natl Acad Sci U S A*, *74*, 5099-5103. https://doi.org/10.1073/pnas.74.11.5099

Gozalo, A., Duke, A., Lan, Y., Pascual-Garcia, P., Talamas, J. A., Nguyen, S. C., Shah, P. P., Jain, R., Joyce, E. F., & Capelson, M. (2020). Core Components of the Nuclear Pore Bind Distinct States of Chromatin and Contribute to Polycomb Repression. *Mol Cell*, *77*, 67-81 e67. https://doi.org/10.1016/j.molcel.2019.10.017

Hao, S., Gestrich, J. Y., Zhang, X., Xu, M., Wang, X., Liu, L., & Wei, H. (2021). Neurotransmitters Affect Larval Development by Regulating the Activity of Prothoracicotropic Hormone-Releasing Neurons in Drosophila melanogaster. *Front Neurosci*, *15*, 653858. https://doi.org/10.3389/fnins.2021.653858

Hayashi, D., Tanabe, K., Katsube, H., & Inoue, Y. H. (2016). B-type nuclear lamin and the nuclear pore complex Nup107-160 influences maintenance of the spindle envelope required for cytokinesis in Drosophila male meiosis. *Biol Open*, *5*, 1011-1021. https://doi.org/10.1242/bio.017566

He, Q., Zhang, Y., Zhang, X., Xu, D., Dong, W., Li, S., & Wu, R. (2017). Nucleoporin Nup358 facilitates nuclear import of Methoprene-tolerant (Met) in an importin beta- and Hsp83-dependent manner. *Insect Biochem Mol Biol*, *81*, 10-18. https://doi.org/10.1016/j.ibmb.2016.12.005

Iglesias, N., Paulo, J. A., Tatarakis, A., Wang, X., Edwards, A. L., Bhanu, N. V., Garcia, B. A., Haas, W., Gygi, S. P., & Moazed, D. (2020). Native Chromatin Proteomics Reveals a Role for Specific Nucleoporins in Heterochromatin Organization and Maintenance. *Mol Cell*, *77*, 51-66 e58. https://doi.org/10.1016/j.molcel.2019.10.018

Jenni, S., Goyal, Y., von Grotthuss, M., Shvartsman, S. Y., & Klein, D. E. (2015). Structural Basis of Neurohormone Perception by the Receptor Tyrosine Kinase Torso. *Mol Cell*, *60*, 941-952. https://doi.org/10.1016/j.molcel.2015.10.026

Johnson, T. K., Crossman, T., Foote, K. A., Henstridge, M. A., Saligari, M. J., Forbes Beadle, L., Herr, A., Whisstock, J. C., & Warr, C. G. (2013). Torso-like functions independently of Torso to regulate Drosophila growth and developmental timing. *Proc Natl Acad Sci U S A*, *110*, 14688-14692. https://doi.org/10.1073/pnas.1309780110

Johnston, D. M., Sedkov, Y., Petruk, S., Riley, K. M., Fujioka, M., Jaynes, J. B., & Mazo, A. (2011). Ecdysone- and NO-mediated gene regulation by competing EcR/Usp and E75A nuclear receptors during Drosophila development. *Mol Cell*, *44*, 51-61. https://doi.org/10.1016/j.molcel.2011.07.033

Kalverda, B., Pickersgill, H., Shloma, V. V., & Fornerod, M. (2010). Nucleoporins directly stimulate expression of developmental and cell-cycle genes inside the nucleoplasm. *Cell*, *140*, 360-371. https://doi.org/10.1016/j.cell.2010.01.011

Kannangara, J. R., Mirth, C. K., & Warr, C. G. (2021). Regulation of ecdysone production in Drosophila by neuropeptides and peptide hormones. *Open Biol*, *11*, 200373. https://doi.org/10.1098/rsob.200373

Kim, S. Y., Kang, H. T., Choi, H. R., & Park, S. C. (2010). Reduction of Nup107 attenuates the growth factor signaling in the senescent cells. *Biochem Biophys Res Commun*, *401*, 131-136. https://doi.org/10.1016/j.bbrc.2010.09.025

Konogami, T., Yang, Y., Ogihara, M. H., Hikiba, J., Kataoka, H., & Saito, K. (2016). Ligand-dependent responses of the silkworm prothoracicotropic hormone receptor, Torso, are maintained by unusual intermolecular disulfide bridges in the transmembrane region. *Sci Rep*, *6*, 22437. https://doi.org/10.1038/srep22437

Kozlova, T., & Thummel, C. S. (2002). Spatial patterns of ecdysteroid receptor activation during the onset of Drosophila metamorphosis. *Development*, *129*, 1739-1750. https://doi.org/10.1242/dev.129.7.1739

Kuhn, T. M., Pascual-Garcia, P., Gozalo, A., Little, S. C., & Capelson, M. (2019). Chromatin targeting of nuclear pore proteins induces chromatin decondensation. *J Cell Biol*, *218*, 2945-2961. https://doi.org/10.1083/jcb.201807139

Lenaerts, C., Marchal, E., Peeters, P., & Vanden Broeck, J. (2019). The ecdysone receptor complex is essential for the reproductive success in the female desert locust, Schistocerca gregaria. *Sci Rep*, *9*, 15. https://doi.org/10.1038/s41598-018-36763-9

Lin, D. H., & Hoelz, A. (2019). The Structure of the Nuclear Pore Complex (An Update). *Annu Rev Biochem*, *88*, 725-783. https://doi.org/10.1146/annurev-biochem-062917-011901

Luo, X., Zhang, J., Zhang, C., & Zhou, N. (2024). PTTH-Torso Signaling System Controls Developmental Timing, Body Size, and Reproduction through Regulating Ecdysone Homeostasis in the Brown Planthopper, Nilaparvata lugens. *Int J Mol Sci*, *25*. https://doi.org/10.3390/ijms25105138

McBrayer, Z., Ono, H., Shimell, M., Parvy, J. P., Beckstead, R. B., Warren, J. T., Thummel, C. S., Dauphin-Villemant, C., Gilbert, L. I., & O'Connor, M. B. (2007). Prothoracicotropic hormone regulates developmental timing and body size in Drosophila. *Dev Cell*, *13*, 857-871. https://doi.org/10.1016/j.devcel.2007.11.003

Mehta, S. J. K., Joshi, P. A., & Mishra, R. K. (2021). Molecular and Phenotypic Characterization Following RNAi Mediated Knockdown in Drosophila. *Bio Protoc*, *11*, e3924. https://doi.org/10.21769/BioProtoc.3924

Mehta, S. J. K., Kumar, V., & Mishra, R. K. (2020). Drosophila ELYS regulates Dorsal dynamics during development. *J Biol Chem*, *295*, 2421-2437. https://doi.org/10.1074/jbc.RA119.009451

Mishra, R. K., Chakraborty, P., Arnaoutov, A., Fontoura, B. M., & Dasso, M. (2010). The Nup107-160 complex and gamma-TuRC regulate microtubule polymerization at kinetochores. *Nat Cell Biol*, *12*, 164-169. https://doi.org/10.1038/ncb2016

Miyake, N., Tsukaguchi, H., Koshimizu, E., Shono, A., Matsunaga, S., Shiina, M., Mimura, Y., Imamura, S., Hirose, T., Okudela, K., Nozu, K., Akioka, Y., Hattori, M., Yoshikawa, N., Kitamura, A., Cheong, H. I., Kagami, S., Yamashita, M., Fujita, A., . . . Matsumoto, N. (2015). Biallelic Mutations in Nuclear Pore Complex Subunit NUP107 Cause Early-Childhood-Onset Steroid-Resistant Nephrotic Syndrome. *Am J Hum Genet*, *97*, 555-566. https://doi.org/10.1016/j.ajhg.2015.08.013

Morchoisne-Bolhy, S., Geoffroy, M. C., Bouhlel, I. B., Alves, A., Auduge, N., Baudin, X., Van Bortle, K., Powers, M. A., & Doye, V. (2015). Intranuclear dynamics of the Nup107-160 complex. *Mol Biol Cell*, *26*, 2343-2356. https://doi.org/10.1091/mbc.E15-02-0060

Niwa, R., & Niwa, Y. S. (2014). Enzymes for ecdysteroid biosynthesis: their biological functions in insects and beyond. *Biosci Biotechnol Biochem*, *78*, 1283-1292. https://doi.org/10.1080/09168451.2014.942250

Ou, Q., Zeng, J., Yamanaka, N., Brakken-Thal, C., O'Connor, M. B., & King-Jones, K. (2016). The Insect Prothoracic Gland as a Model for Steroid Hormone Biosynthesis and Regulation. *Cell Rep*, *16*, 247-262. https://doi.org/10.1016/j.celrep.2016.05.053

Rewitz, K. F., Yamanaka, N., Gilbert, L. I., & O'Connor, M. B. (2009). The insect neuropeptide PTTH activates receptor tyrosine kinase torso to initiate metamorphosis. *Science*, *326*(5958), 1403-1405. https://doi.org/10.1126/science.1176450

Rewitz, K. F., Yamanaka, N., & O'Connor, M. B. (2013). Developmental checkpoints and feedback circuits time insect maturation. *Curr Top Dev Biol*, *103*, 1-33. https://doi.org/10.1016/B978-0-12-385979-2.00001-0

Rout, M. P., Aitchison, J. D., Suprapto, A., Hjertaas, K., Zhao, Y., & Chait, B. T. (2000). The yeast nuclear pore complex: composition, architecture, and transport mechanism. *J Cell Biol*, *148*, 635-651. https://doi.org/10.1083/jcb.148.4.635

Shimell, M., Pan, X., Martin, F. A., Ghosh, A. C., Leopold, P., O'Connor, M. B., & Romero, N. M. (2018). Prothoracicotropic hormone modulates environmental adaptive plasticity through the control of developmental timing. *Development*, *145*. https://doi.org/10.1242/dev.159699

Shore, T., Levi, T., Kalifa, R., Dreifuss, A., Rekler, D., Weinberg-Shukron, A., Nevo, Y., Bialistoky, T., Moyal, V., Gold, M. Y., Leebhoff, S., Zangen, D., Deshpande, G., & Gerlitz, O. (2022). Nucleoporin107 mediates female sexual differentiation via Dsx. *Elife*, *11*. https://doi.org/10.7554/eLife.72632

Sopko, R., & Perrimon, N. (2013). Receptor tyrosine kinases in Drosophila development. *Cold Spring Harb Perspect Biol*, *5*. https://doi.org/10.1101/cshperspect.a009050

Tennessen, J. M., & Thummel, C. S. (2011). Coordinating growth and maturation - insights from Drosophila. *Curr Biol*, *21*, R750-757. https://doi.org/10.1016/j.cub.2011.06.033

Varghese, J., & Cohen, S. M. (2007). microRNA miR-14 acts to modulate a positive autoregulatory loop controlling steroid hormone signaling in Drosophila. *Genes Dev*, *21*, 2277-2282. https://doi.org/10.1101/gad.439807

Walther, T. C., Alves, A., Pickersgill, H., Loiodice, I., Hetzer, M., Galy, V., Hulsmann, B. B., Kocher, T., Wilm, M., Allen, T., Mattaj, I. W., & Doye, V. (2003). The conserved Nup107-160 complex is critical for nuclear pore complex assembly. *Cell*, *113*, 195-206. https://doi.org/10.1016/s0092-8674(03)00235-6

Weinberg-Shukron, A., Renbaum, P., Kalifa, R., Zeligson, S., Ben-Neriah, Z., Dreifuss, A., Abu-Rayyan, A., Maatuk, N., Fardian, N., Rekler, D., Kanaan, M., Samson, A. O., Levy-Lahad, E., Gerlitz, O., & Zangen, D. (2015). A mutation in the nucleoporin-107 gene causes XX gonadal dysgenesis. *J Clin Invest*, *125*, 4295-4304. https://doi.org/10.1172/JCI83553

Yamanaka, N., Rewitz, K. F., & O'Connor, M. B. (2013). Ecdysone control of developmental transitions: lessons from Drosophila research. *Annu Rev Entomol*, *58*, 497-516. https://doi.org/10.1146/annurev-ento-120811-153608

Zheng, X., Yang, S., Han, Y., Zhao, X., Zhao, L., Tian, T., Tong, J., Xu, P., Xiong, C., & Meng, A. (2012). Loss of zygotic NUP107 protein causes missing of pharyngeal skeleton and other tissue defects with impaired nuclear pore function in zebrafish embryos. *J Biol Chem*, *287*, 38254-38264. https://doi.org/10.1074/jbc.M112.408997

Zuccolo, M., Alves, A., Galy, V., Bolhy, S., Formstecher, E., Racine, V., Sibarita, J. B., Fukagawa, T., Shiekhattar, R., Yen, T., & Doye, V. (2007). The human Nup107-160 nuclear pore subcomplex contributes to proper kinetochore functions. *EMBO J*, *26*, 1853-1864. https://doi.org/10.1038/sj.emboj.7601642

Figures

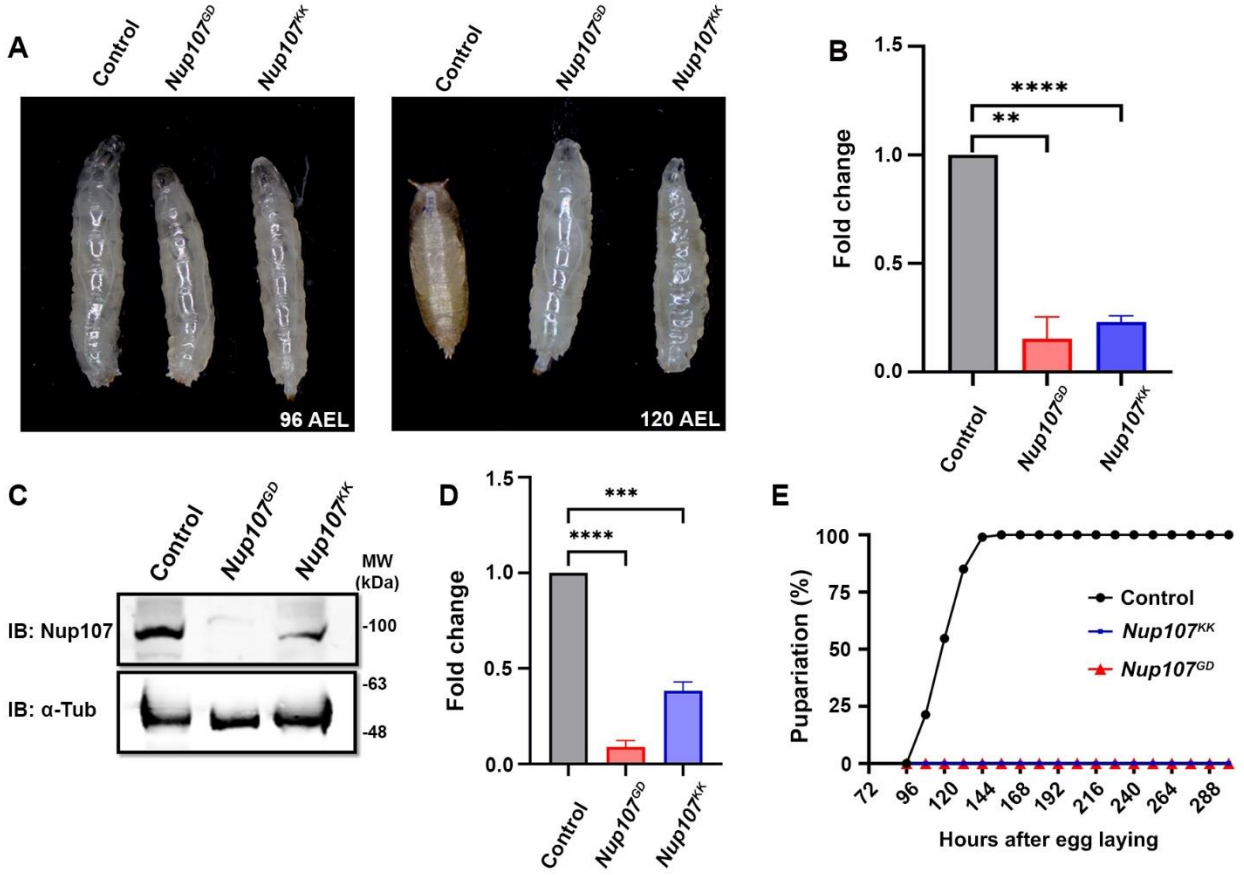

Figure 1. *Nup107* depletion impairs metamorphosis.

(A) Growth profile of third instar larvae from *Actin5C-Gal4* driven control and *Nup107* knockdowns (*Nup107*^{GD} and *Nup107*^{KK} RNAi lines) at 96 h AEL (after egg laying) and 120 h AEL.

(B) Quantitation of *Nup107* knockdown efficiency. Data are represented from at least three independent experiments. Statistical significance was derived from the Student's t-test. Error bars represent SEM. ***p* = <0.001 and ****p* = <0.0001.

(C) Immunodetection of Nup107 protein levels in third instar larval brain-complex lysates from control and *Nup107* knockdown.

(D) Quantification of Nup107 protein levels seen in (C). Data are represented from at least three independent experiments. Statistical significance was derived from the Student's t-test. Error bars represent SEM. ***p = <0.0002 and ****p = <0.0001.

(E) Comparison of pupariation profiles of control and *Nup107* knockdown organisms.

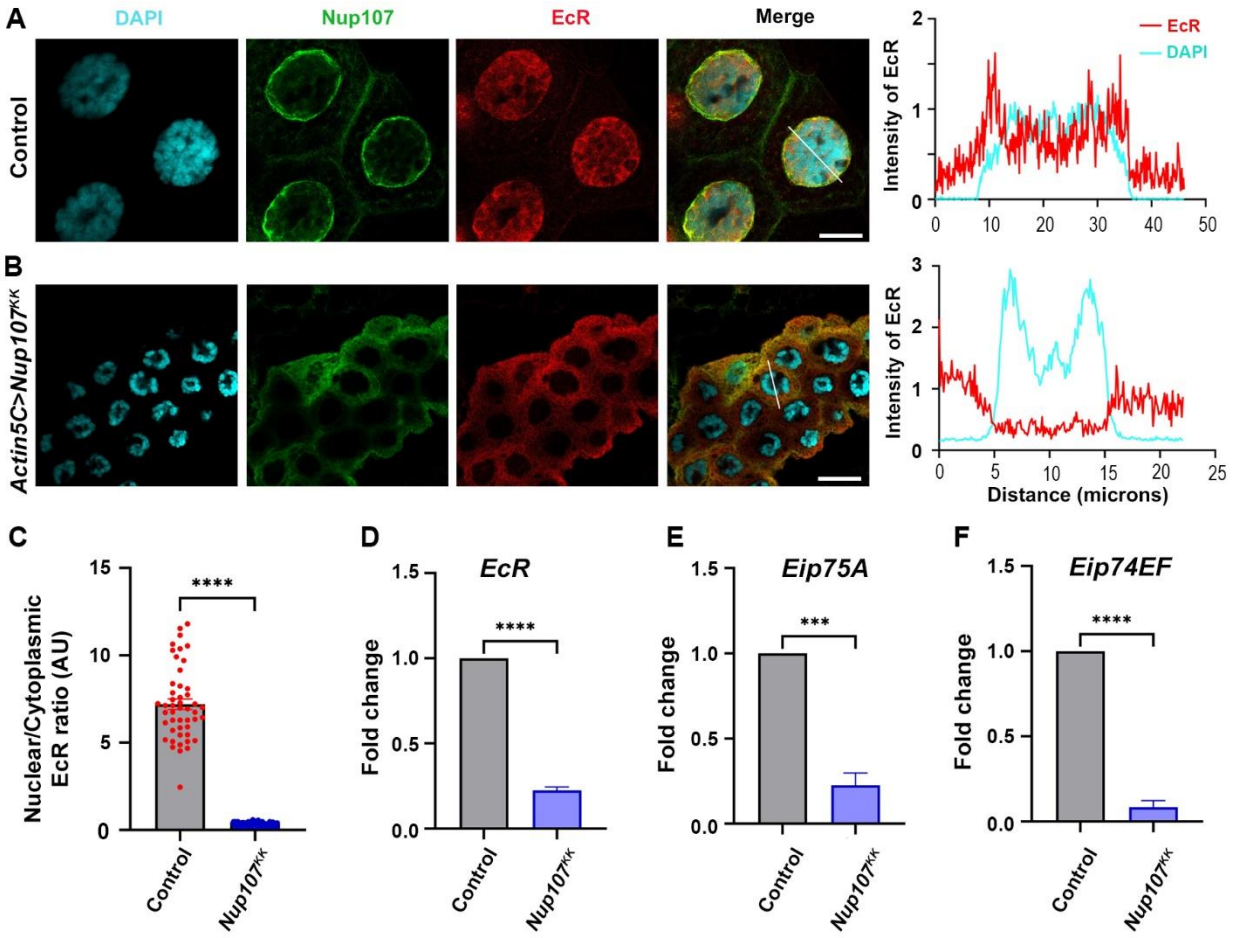

Figure 2. Ubiquitous knockdown of *Nup107* disrupts ecdysone signaling.

(A-B) Staining of third instar larval salivary glands from control (A) and ubiquitous *Nup107* knockdown (B) with Ecdysone receptor (anti-EcR antibody, red) and Nup107 (anti-Nup107 antibody, green). DNA is stained with DAPI. Scale bars, 20 µm. Charts represent the line scan intensity profile of EcR (Red) and DAPI (Cyan) in the salivary gland nucleus region.

(C) Quantification of the nucleocytoplasmic ratio of EcR under control and *Nup107* knockdown conditions. At least 45 nuclei were analyzed from 7 to 8 pairs of salivary glands. Statistical significance was derived from the Student's t-test. Error bars represent SEM. ****p = < 0.0001.

(D-F) Analysis of ecdysone-inducible genes, *EcR* (D), *Eip75A* (E), and *Eip74EF* (F) expression, respectively, at the onset of metamorphosis (late third instar larvae stage).

Data are represented from at least three independent experiments. Statistical significance was derived from the Student's t-test. The error bars represent the SEM. ***p = <0.0004 and ****p = <0.0001.

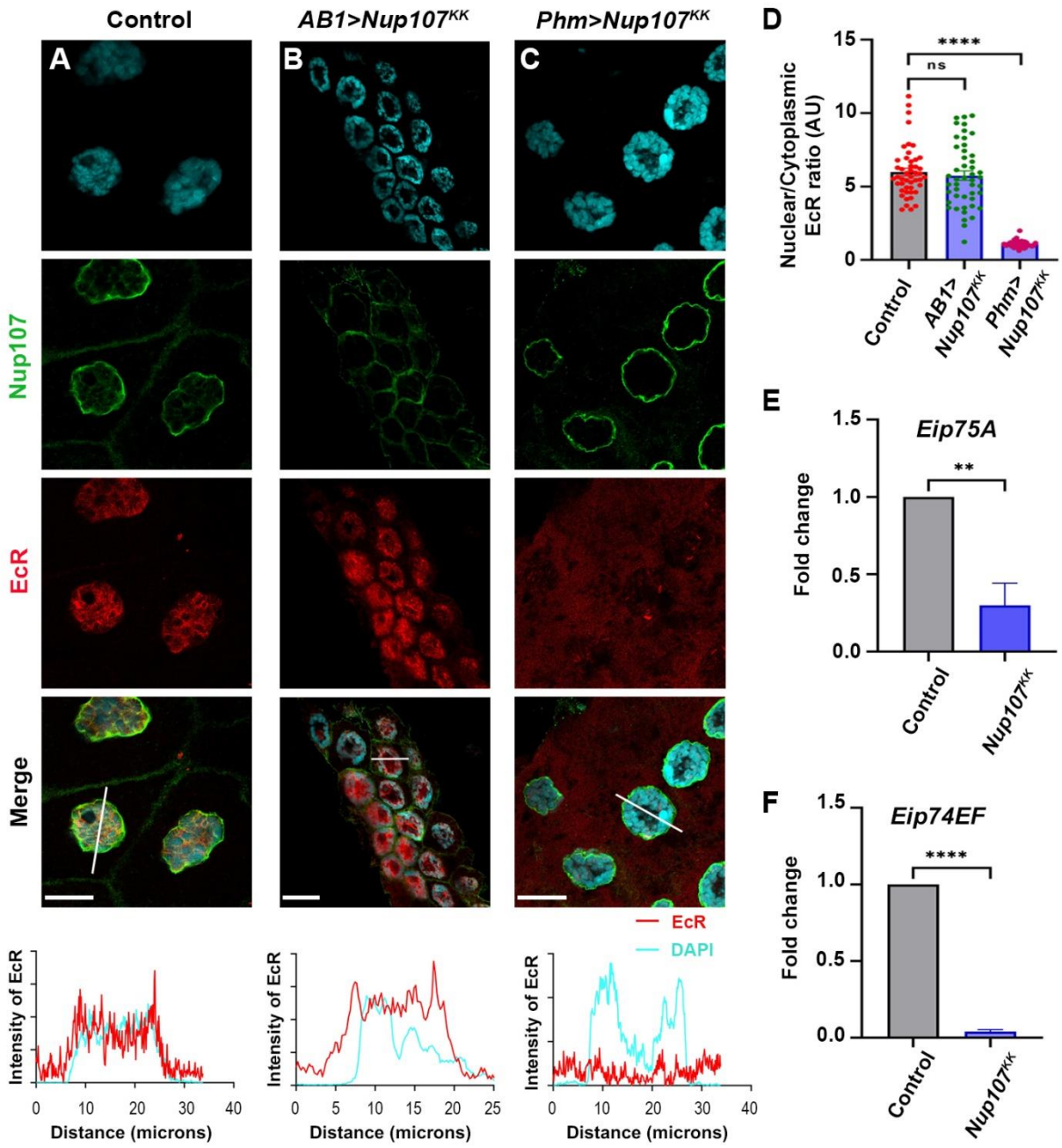

Figure 3. *Nup107* regulates Ecdysone receptor-dependent signaling.

(A-C) Detection of and quantitation of nucleocytoplasmic distribution of EcR (anti-EcR antibody, red) and Nup107 (anti-Nup107 antibody, green) in control (A), salivary gland-specific *Nup107* depletion (B), and prothoracic gland-specific *Nup107* depletion (C) from third instar larval salivary gland nuclei. DNA is stained with DAPI. Scale bars, 20 μm.

Charts represent the line scan intensity profile of EcR (Red) and DAPI (Cyan) in the salivary gland nucleus region.

(D) EcR nucleo-cytoplasmic quantification ratio from the salivary gland and prothoracic gland-specific *Nup107* knockdown, respectively. At least 45 nuclei were analyzed from 7 to 8 pairs of salivary glands. Statistical significance was derived from the Student's t-test. Error bars represent SEM. ****p = <0.0001, and ns is non-significant.

(E-F) Quantitation of expression of *Eip75A* (E) and *Eip74EF* (F) ecdysone-inducible genes at the onset of metamorphosis (RNA isolated from late third instar larvae of control and prothoracic gland-specific *Nup107* depletion). Data are represented from at least three independent experiments. Statistical significance was derived from the Student's t-test. Error bars represent SEM. **p = <0.008 and ****p = <0.0001.

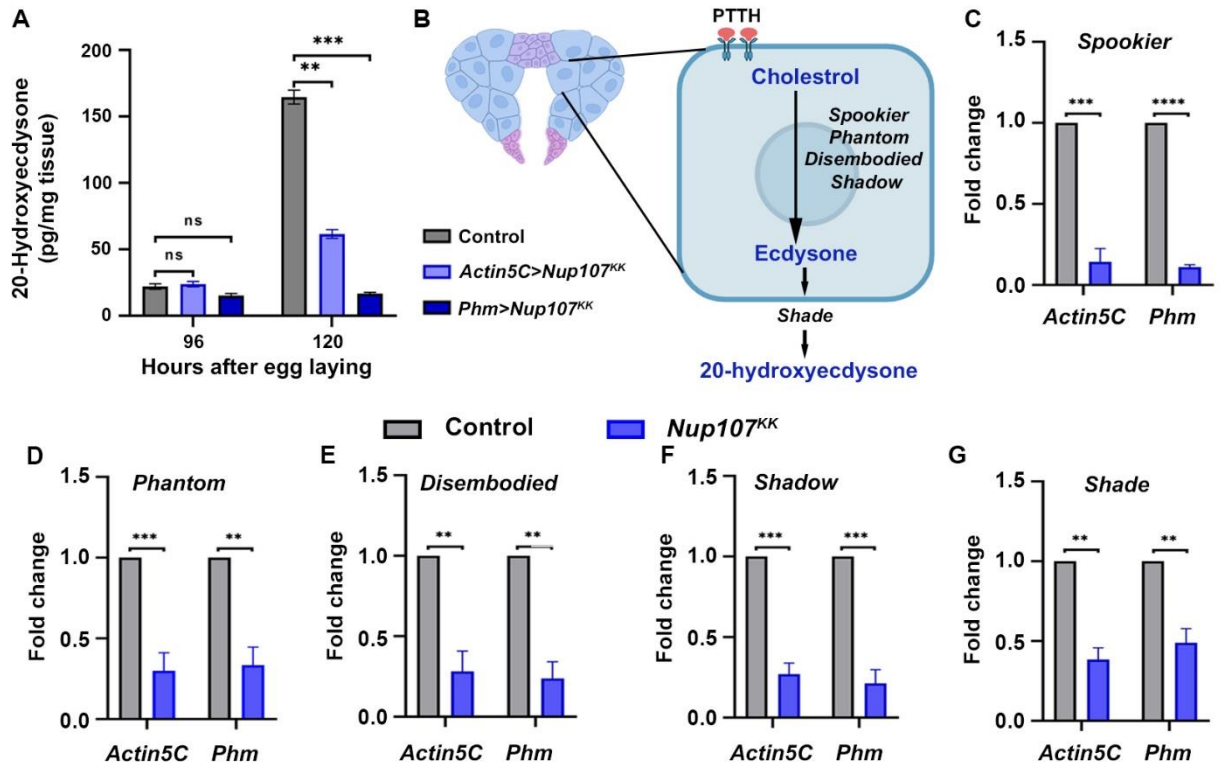

Figure 4. *Nup107* critically regulates the expression of ecdysone-biosynthetic genes.

(A) ELISA measurements of whole-body 20-hydroxyecdysone (20E) levels in control, ubiquitous (*Actin5C-Gal4*), and prothoracic gland-specific (*Phm-Gal4*) *Nup107* depletion at 96 and 120 h AEL. Data are represented from at least three independent experiments. Statistical significance was derived from the Student's t-test. Error bars represent SEM. ***p* = <0.0013, ****p* = < 0.0009 and ns is non-significant.

(B) Schematic representation of a Prothoracic gland cell showing genes involved in ecdysone biosynthesis from cholesterol.

(C-G) Quantification of ecdysone-biosynthetic gene expression levels of *Spookier* (C), *Phantom* (D), *Disembodied* (E), *Shadow* (F), and *Shade* (G) in cDNA isolated from control, and *Nup107* knockdown late third instar larvae. Data are represented from at least three independent experiments. Statistical significance was derived from the Student's t-test. Error bars represent SEM. ***p* = <0.001, ****p* = <0.0005 and, *****p* = <0.0001.

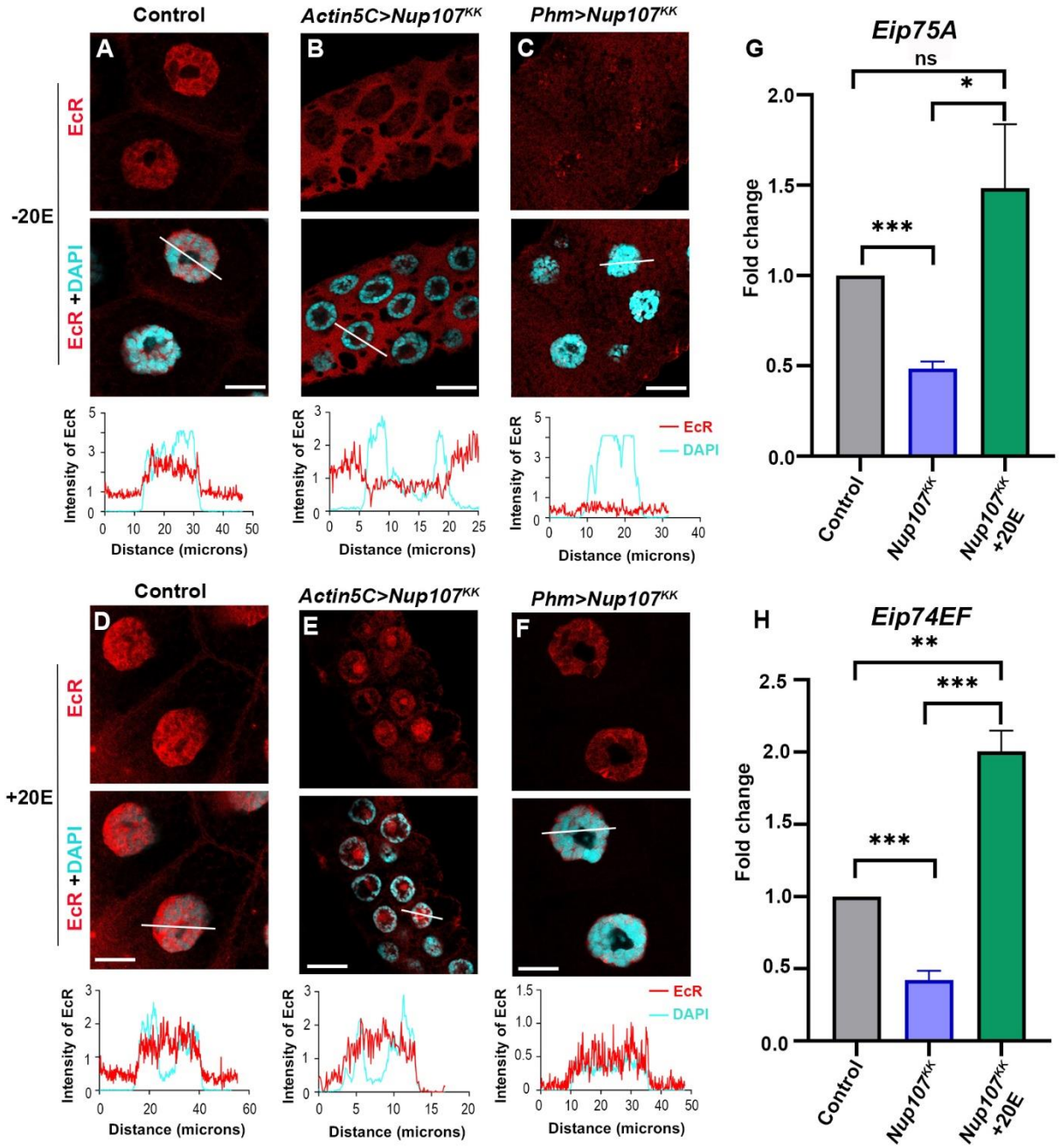

Figure 5. 20E supplementation rescues *Nup107* depletion-specific EcR signaling defects.

(A-F) Visualization of the nucleocytoplasmic distribution of EcR (anti-EcR antibody, red) without 20E (A-C) and with 20E (D-F) treatment in larval salivary glands of control, ubiquitous (*Actin5C-Gal4*) *Nup107* knockdown, and prothoracic gland-specific (*Phm-*

Gal4) *Nup107* knockdown. DNA is stained with DAPI. Scale bars, 20 µm. Charts represent the line scan intensity profile of EcR (Red) and DAPI (Cyan) in the salivary gland nucleus region.

(G-H) Comparative quantification of expression ecdysone-inducible genes *Eip75A* (G) and *Eip74EF* (H) from 20E treated salivary glands. Data are represented from at least three independent experiments. Statistical significance was derived from the Student's t-test. Error bars represent SEM. *p = <0.02, **p = <0.002, ***p = <0.0008 and ns is non-significant.

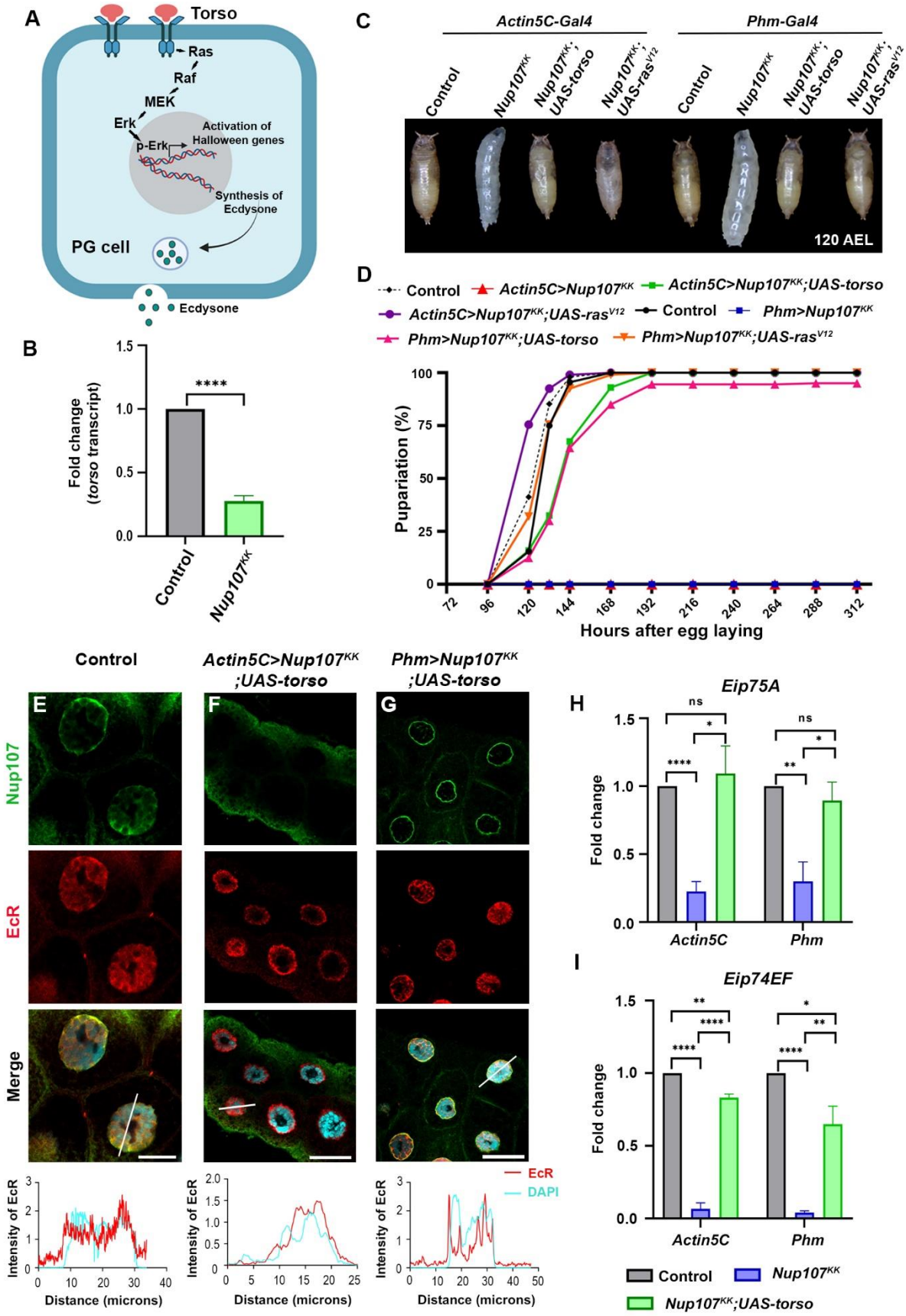
A
Torso
Ras
Raf
MEK
Erk
p-Erk
Activation of Halloween genes
Synthesis of Ecdysone
PG cell
Ecdysone
B
Fold change (torso transcript)
****
Control
Nup107KK
C
Actin5C-Gal4
Phm-Gal4
Control
Nup107KK
Nup107KK; UAS-torso
Nup107KK; UAS-rasV12
120 AEL
D
Control
Actin5C>Nup107KK
Actin5C>Nup107KK;UAS-torso
Actin5C>Nup107KK;UAS-rasV12
Phm>Nup107KK
Phm>Nup107KK;UAS-torso
Phm>Nup107KK;UAS-rasV12
Puparation (%)
Hours after egg laying
Control
Actin5C>Nup107KK ;UAS-torso
Phm>Nup107KK ;UAS-torso
E
F
G
Nup107
EcR
Merge
Intensity of EcR
Distance (microns)
EcR
DAPI
H
Eip75A
Fold change
ns
*
****
**
Actin5C
Phm
I
Eip74EF
Control
Nup107KK
Nup107KK;UAS-torso

Figure 6. *Torso* and *Nup107* act synergistically to activate the ecdysone signaling.

(A) A model of the Torso pathway and its components.

(B) Quantitation of *torso* transcript levels from control and *Nup107* depleted larvae (ubiquitous depletion using *Actin5C-Gal4*). Data are represented from at least three independent experiments. Statistical significance was derived from the Student's t-test. Error bars represent SEM. ****p = <0.0001.

(C-D) Comparison of pupariation profiles of control, *Nup107* knockdown, and *torso* and ras^{V12} overexpressing rescue organisms.

(E-G) Detection and quantitation of nucleocytoplasmic distribution of EcR (anti-EcR antibody, red) and Nup107 (anti-Nup107 antibody, green) in control, *torso* overexpressing ubiquitous *Nup107* knockdown (*Actin5C-Gal4>Nup107*^{KK}*; UAS-torso*) and *torso* overexpressing PG-specific *Nup107* knockdown (*Phm-Gal4>Nup107*^{KK}; *UAS-torso*) third instar larval salivary gland nuclei. DNA is stained with DAPI. Scale bars, 20 µm. Charts represent the line scan intensity profile of EcR (Red) and DAPI (Cyan) in the salivary gland nucleus region.

(H-I) Quantification of expression of *Eip75A* (H) and *Eip74EF* (I) ecdysone-inducible genes, respectively. Data are represented from at least three independent experiments. Statistical significance was derived from the Student's t-test. Error bars represent SEM. *p = <0.03, **p = <0.008, ****p = <0.0001 and ns is non-significant.

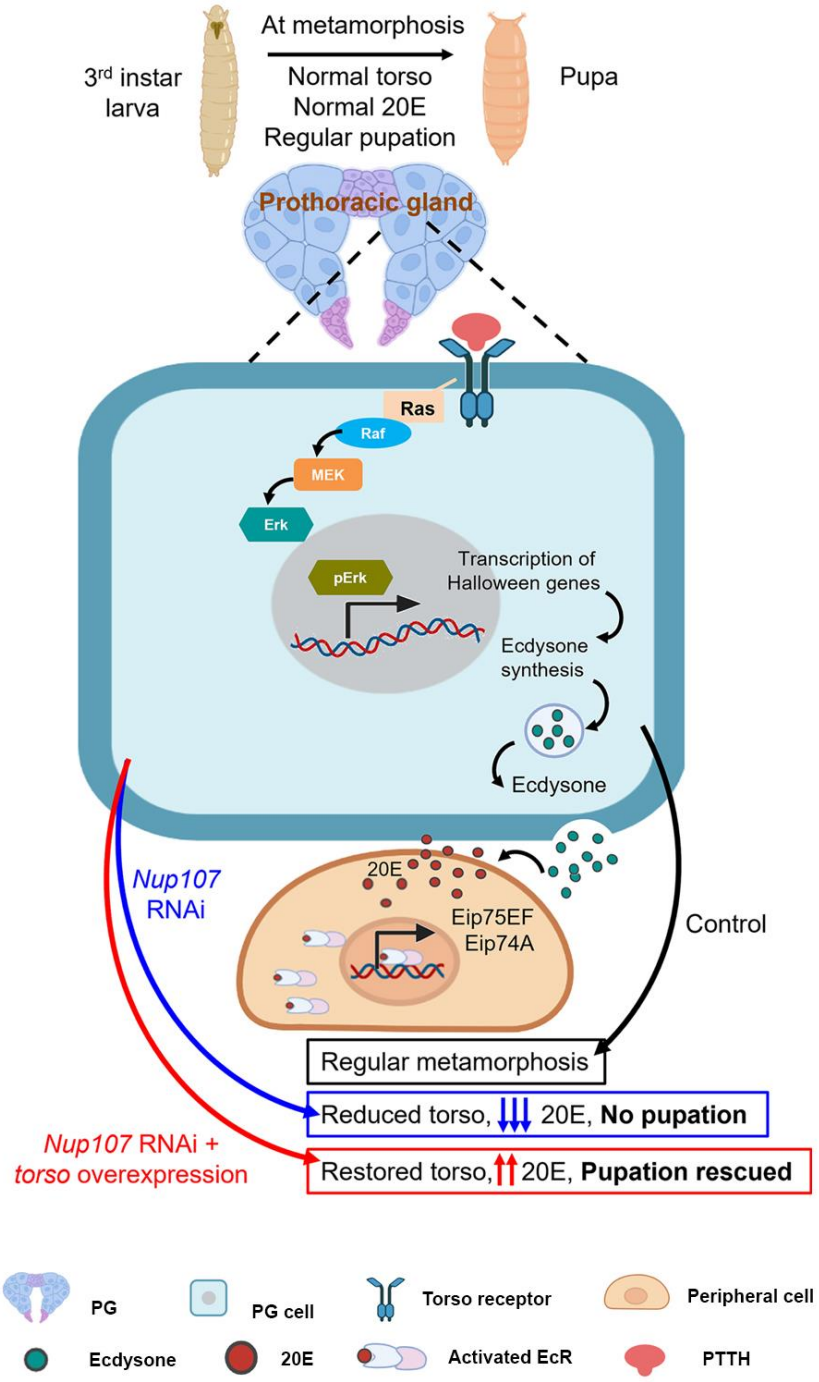

Figure 7. Theoretical Model of Nup107 functions in metamorphosis:

During metamorphosis, the prothoracic gland (PG) responds to prothoracicotropic hormone (PTTH) via Torso receptors. The MAP kinase pathway involving Raf, MEK, and ERK, initiated by Ras, leads to *Halloween* gene expression responsible for Ecdysone synthesis and release. Ecdysone is converted to active 20-hydroxyecdysone

(20E) in peripheral tissues. The binding of 20E to the Ecdysone receptor (EcR) allows EcR nuclear translocation and EcR pathway activation, culminating in target gene expression facilitating the metamorphic transition. Nup107 depletion negatively impacts Torso levels and Torso pathway activation, inducing pupariation arrest, which can be rescued by autonomous activation of the Torso pathway.

Supplementary Information

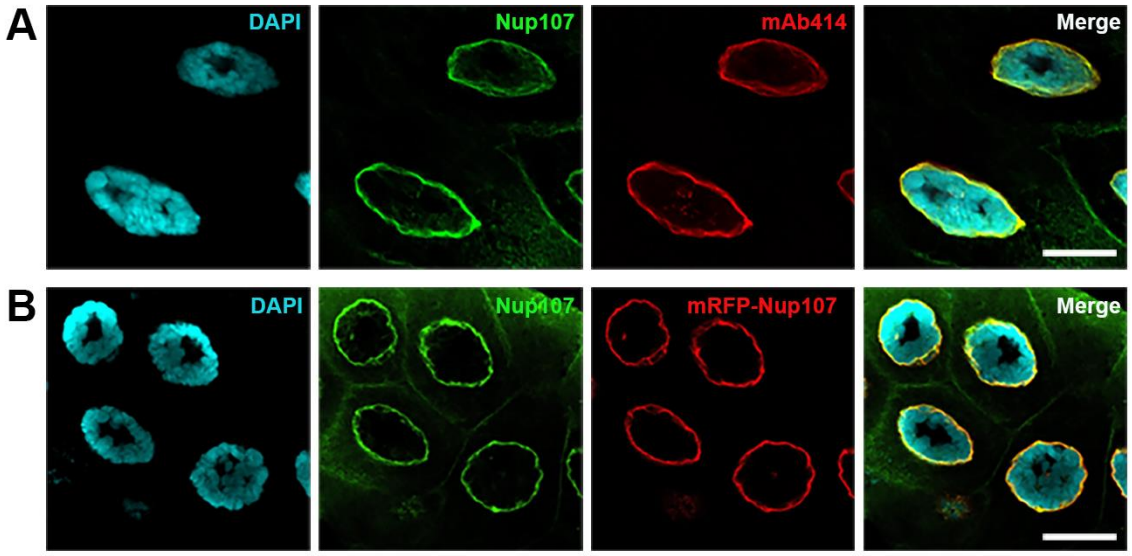

Figure S1. Nup107 staining in salivary glands:

(A-B) Custom-generated polyclonal anti-Nup107 antibody colocalizes with pan-FG-Nup antibody, mAb414 (A), and mRFP-tagged Nup107 (B) at the nuclear rim of the third instar salivary gland. DNA stained with DAPI. Scale bars, 20 µm.

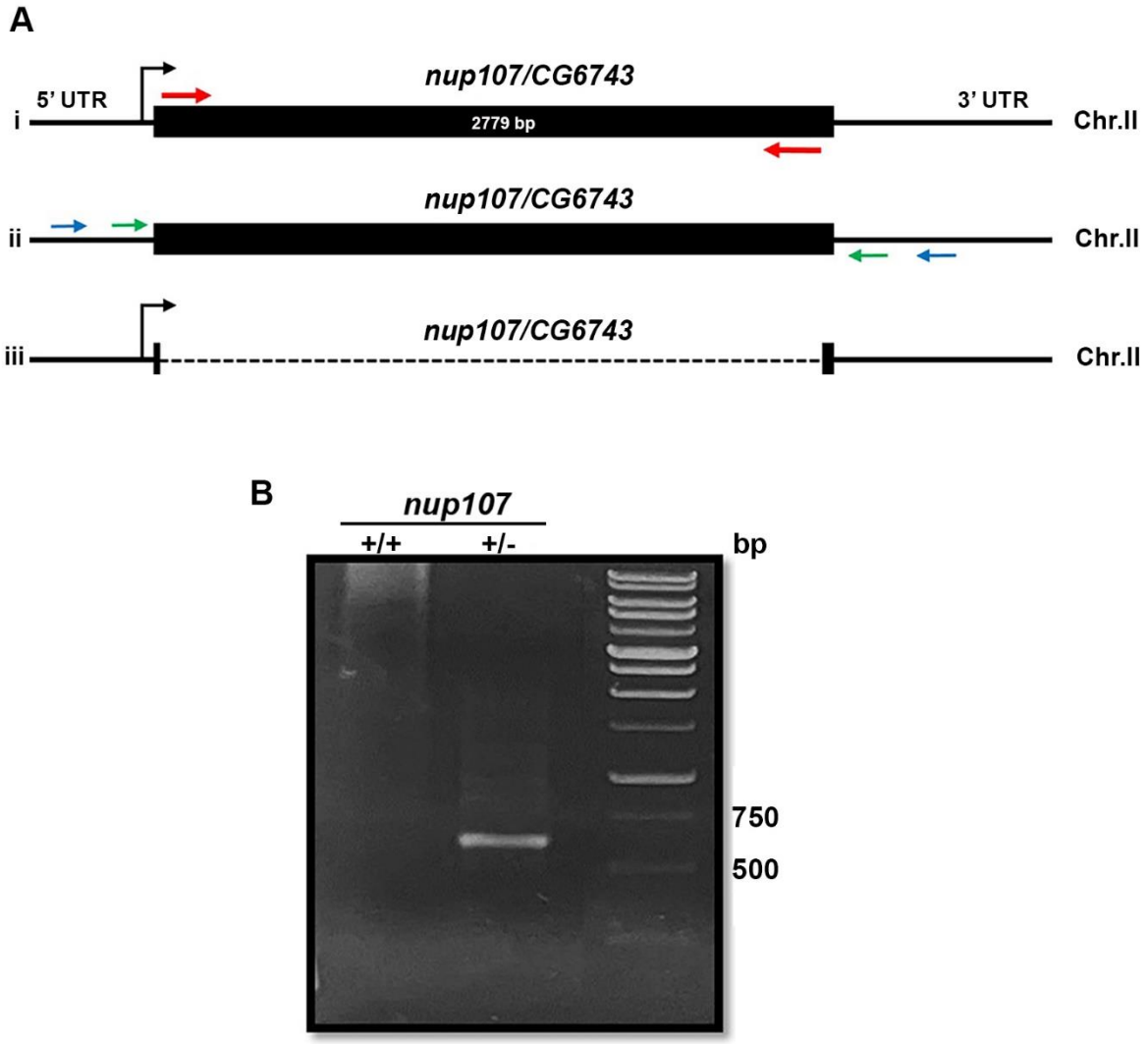

Figure S2. *Nup107* CRISPR mutant generation:

(A) Schematic representation of *Nup107*^{KO} generation. (Ai) The genomic locus of *nup107* on chromosome-II (2L). The filled black box corresponds to the *nup107* ORF (2779 bp) with gRNA(s) positions indicated by red arrows. The first and second gRNAs were designed near start and stop codons, respectively, of the *nup107* locus. (Aii) Blue and green arrows indicate two sets of primers located in the 5'-UTR and 3'-UTR regions used for screening of *Nup107* mutant. (Aiii) The black discontinuous line represents the *nup107* (2752 bp) deletion allele.

(B) Confirmation of *Nup107* deletion mutant (heterozygous) line assessed by the presence of a ~630 bp band amplified from isolated genomic DNA.

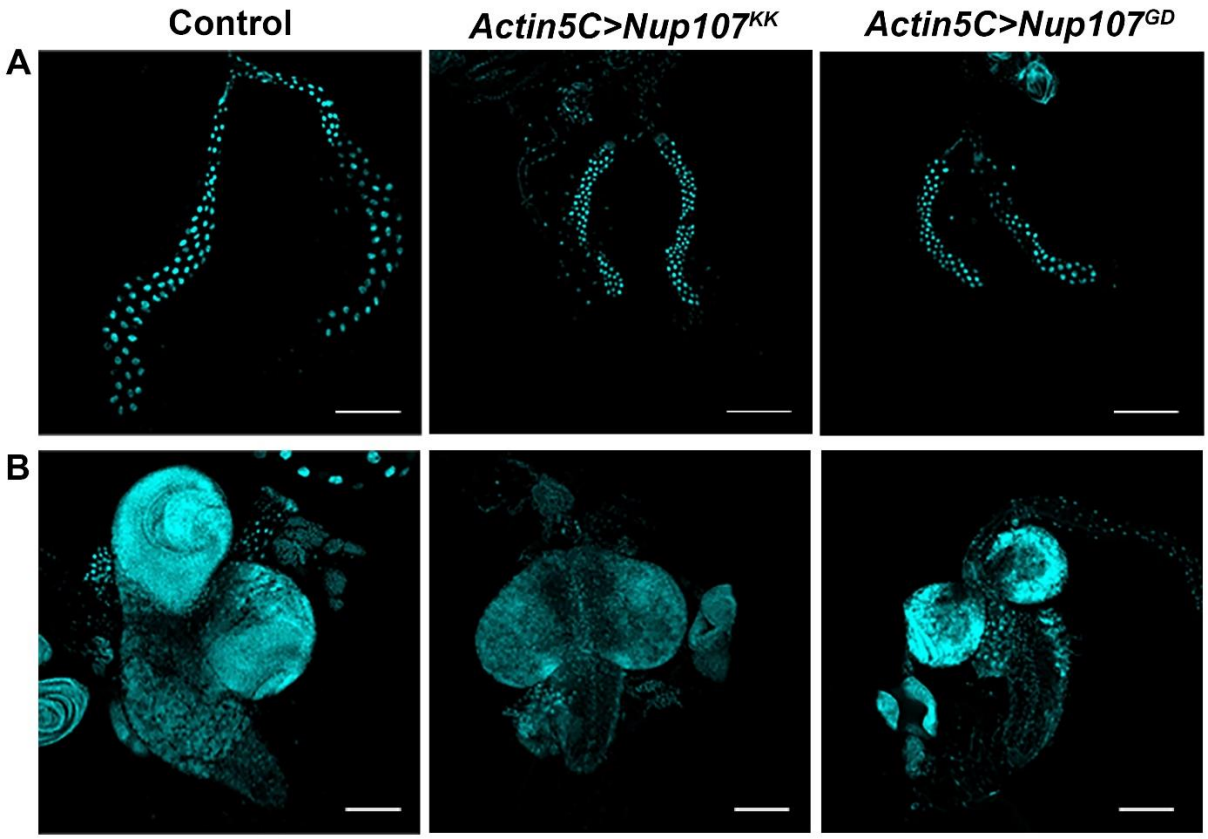

Figure S3. Compromised organ size due to ubiquitous depletion of *Nup107*:

Actin5C-Gal4 was used as a ubiquitous driver.

(A-B) Third instar larval salivary gland (A), and brain complex (B) images of Control, *Nup107*^{KK} RNAi and *Nup107*^{GD} RNAi. DNA stained with DAPI. Scale bars are 200 µm and 100 µm in (A) and (B), respectively.

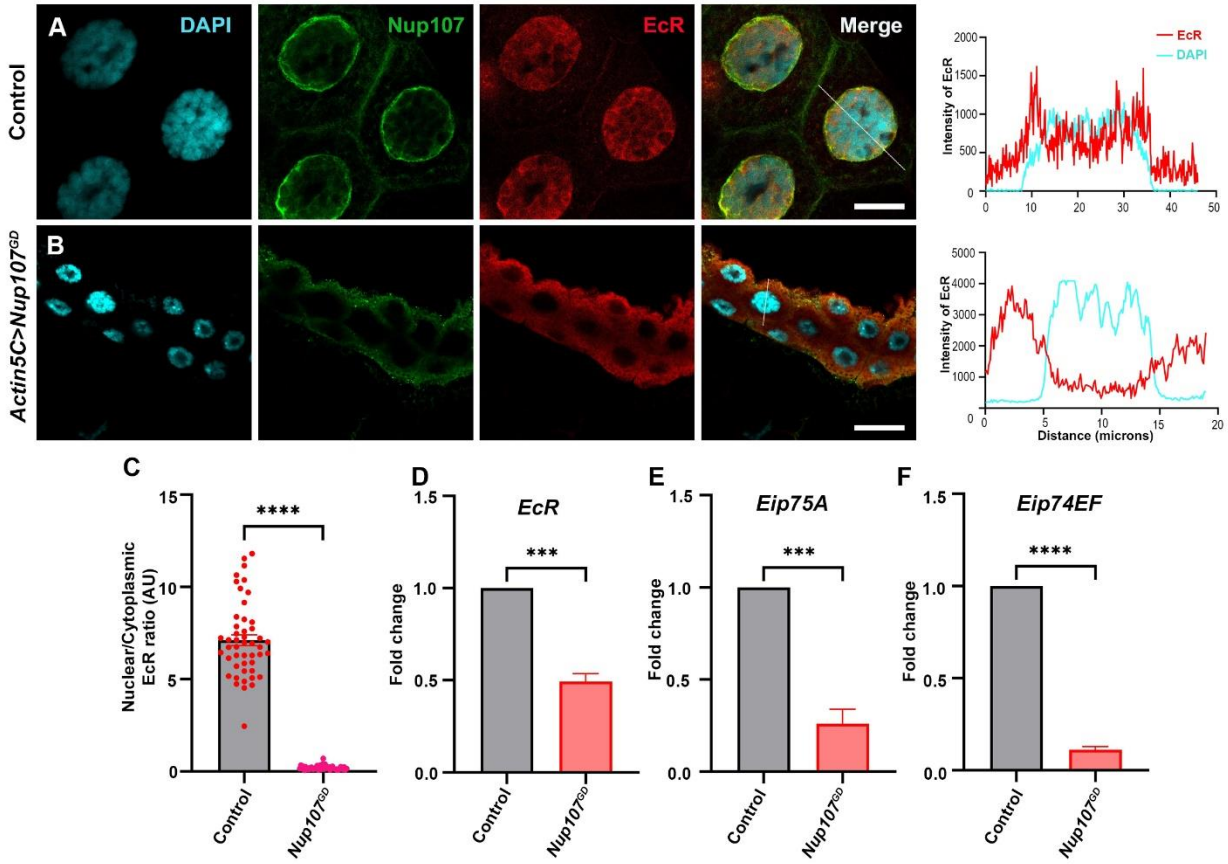

Figure S4. Ubiquitous knockdown of *Nup107* using *Nup107^{GD}* RNAi disrupts ecdysone signaling.

(A-B) Staining of third instar larval salivary glands from control (A) and ubiquitous *Nup107^{GD}* knockdown (B) with Ecdysone receptor (anti-EcR antibody, red) and Nup107 (anti-Nup107 antibody, green). DNA is stained with DAPI, and Scale bars, 20 µm. Charts represent the line scan intensity profile of EcR (Red) and DAPI (Cyan) in the salivary gland nucleus region.

(C) Quantification of nucleo-cytoplasmic ratio of EcR under control and *Nup107* knockdown conditions. At least 45 nuclei were analyzed from 7 to 8 pairs of salivary glands. Statistical significance was derived from the Student's t-test. Error bars represent SEM. ****p = < 0.0001.

(D-F) Analysis of ecdysone-inducible genes, *EcR* (D), *Eip75A* (E) and *Eip74EF* (F) expression. Data are represented from at least three independent experiments.

Statistical significance was derived from the Student's t-test. The error bars represent the SEM. ***p = < 0.0007 and ****p = < 0.0001.

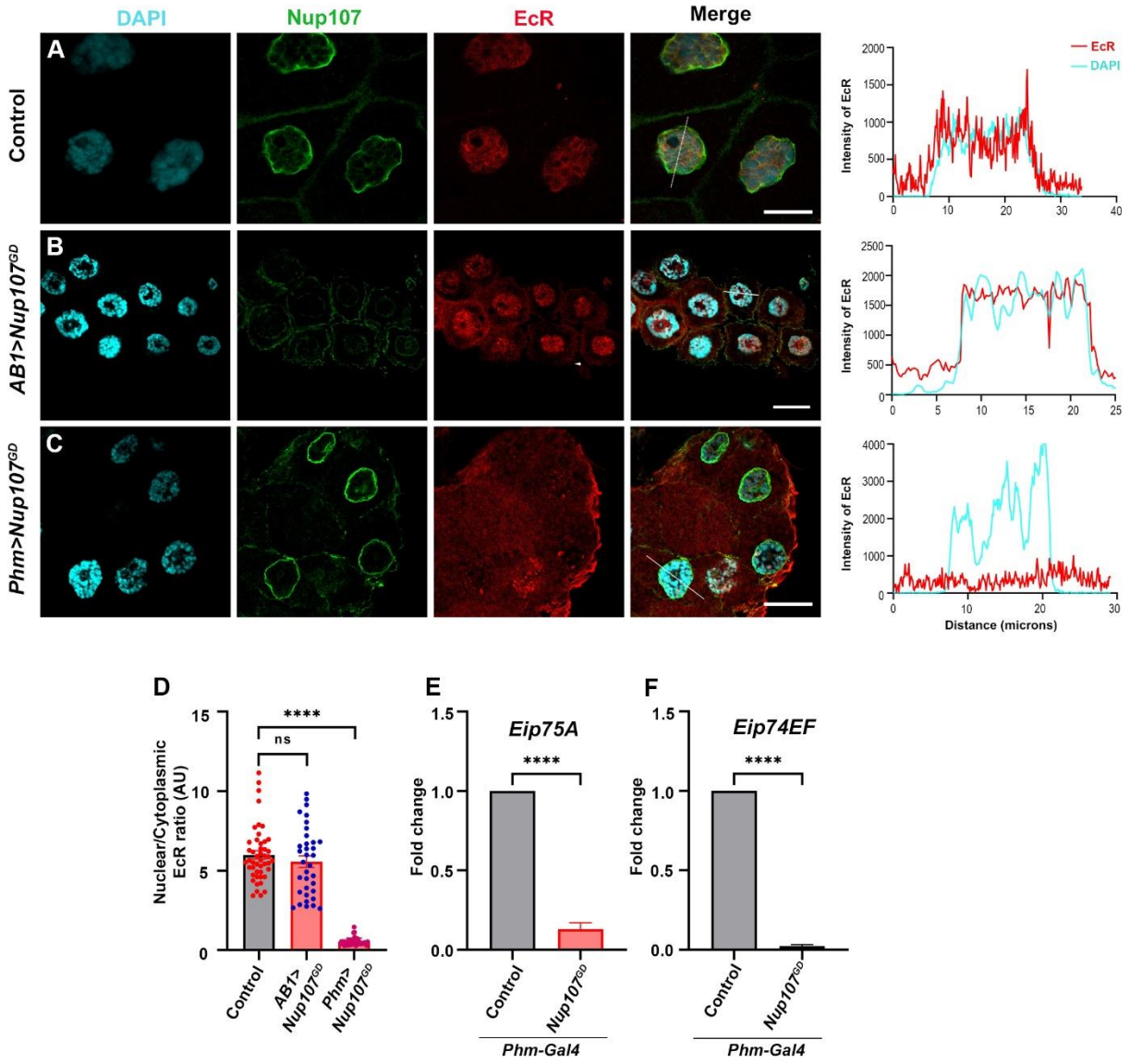

Figure S5. *Nup107^{GD} RNAi mediated Nup107* depletion regulates Ecdysone receptor-dependent signaling.

(A-C) Detection of and quantitation of nucleocytoplasmic distribution of EcR (anti-EcR antibody, red) and Nup107 (anti-Nup107 antibody, green) in control (A), salivary gland-specific *Nup107^{GD}* depletion (B), and prothoracic gland-specific *Nup107^{GD}* depletion (C) from third instar larval salivary gland nuclei. DNA is stained with DAPI. Scale bars, 20 µm. Charts represent the line scan intensity profile of EcR (Red) and DAPI (Cyan) in the salivary gland nucleus region.

(D) EcR nucleo-cytoplasmic quantification ratio from salivary gland, and prothoracic gland-specific *Nup107* knockdown. At least 45 nuclei were analyzed from 7 to 8 pairs of salivary glands. Statistical significance was derived from the Student's t-test. Error bars represent SEM. ****p = < 0.0001 and ns is non-significant.

(E-F) Quantitation of expression of *Eip75A* (E), and *Eip74EF* (F) ecdysone-inducible genes at the onset of metamorphosis (RNA isolated from late third instar larval stage). Data are represented from at least three independent experiments. Statistical significance was derived from the Student's t-test. Error bars represent SEM. ****p = < 0.0001.

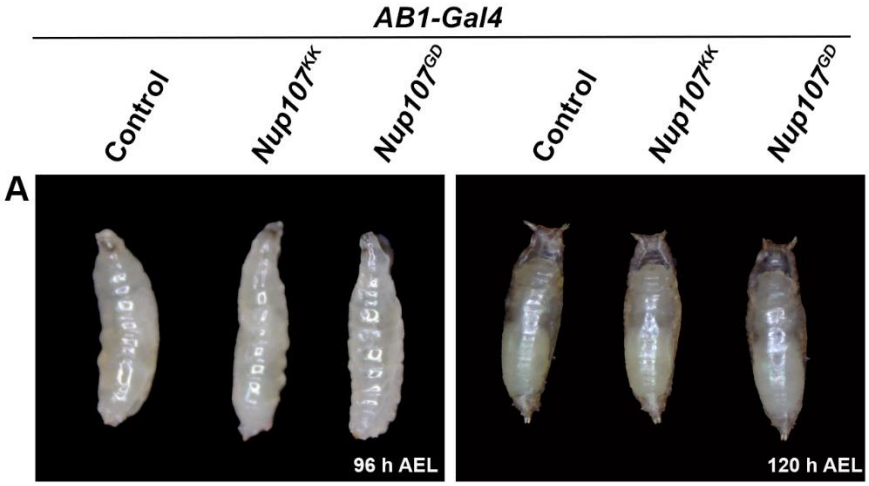
AB1-Gal4
Control
Nup107KK
Nup107GD
Control
Nup107KK
Nup107GD
A
96 h AEL
120 h AEL

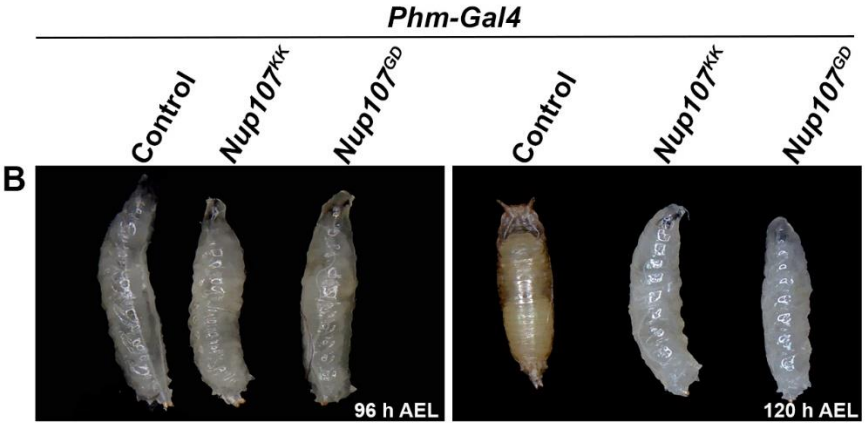
Phm-Gal4
Control
Nup107KK
Nup107GD
Control
Nup107KK
Nup107GD
B
96 h AEL
120 h AEL

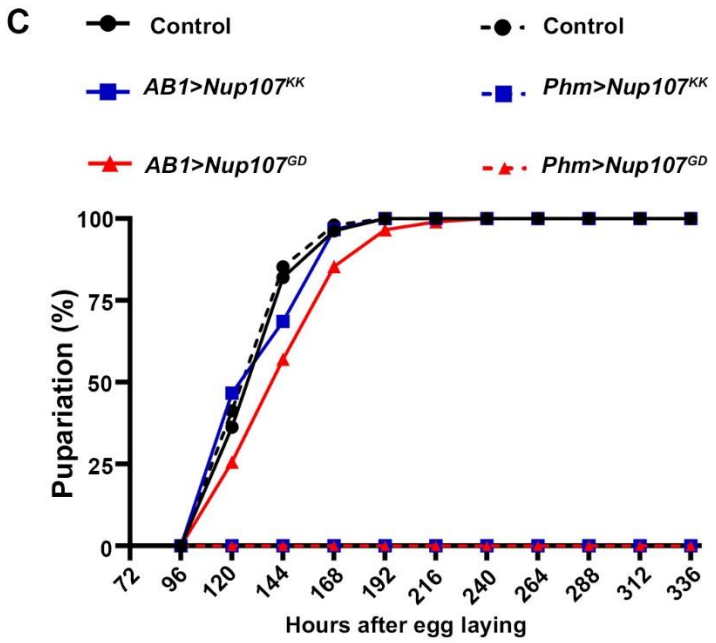
C
Control
Control
AB1>Nup107KK
Phm>Nup107KK
AB1>Nup107GD
Phm>Nup107GD
Pupariation (%)
100
75
50
25
0
72
96
120
144
168
192
216
240
264
288
312
336
Hours after egg laying

Figure S6. *Nup107* regulates metamorphosis via Ecdysone synthesis.

(A) Growth profile of third instar larvae from *AB1-Gal4* driven control and *Nup107* knockdowns (*Nup107*^{KK} and *Nup107*^{GD} RNAi lines) at 96 h AEL (hours after egg laying) and 120 h AEL.

(B) Growth profile of third instar larvae from *Phm-Gal4* driven control and *Nup107* knockdowns (*Nup107*^{KK} and *Nup107*^{GD} RNAi lines) at 96 h AEL and 120 h AEL.

(C) Comparison of pupariation profiles of control, and *Nup107* knockdown organisms.

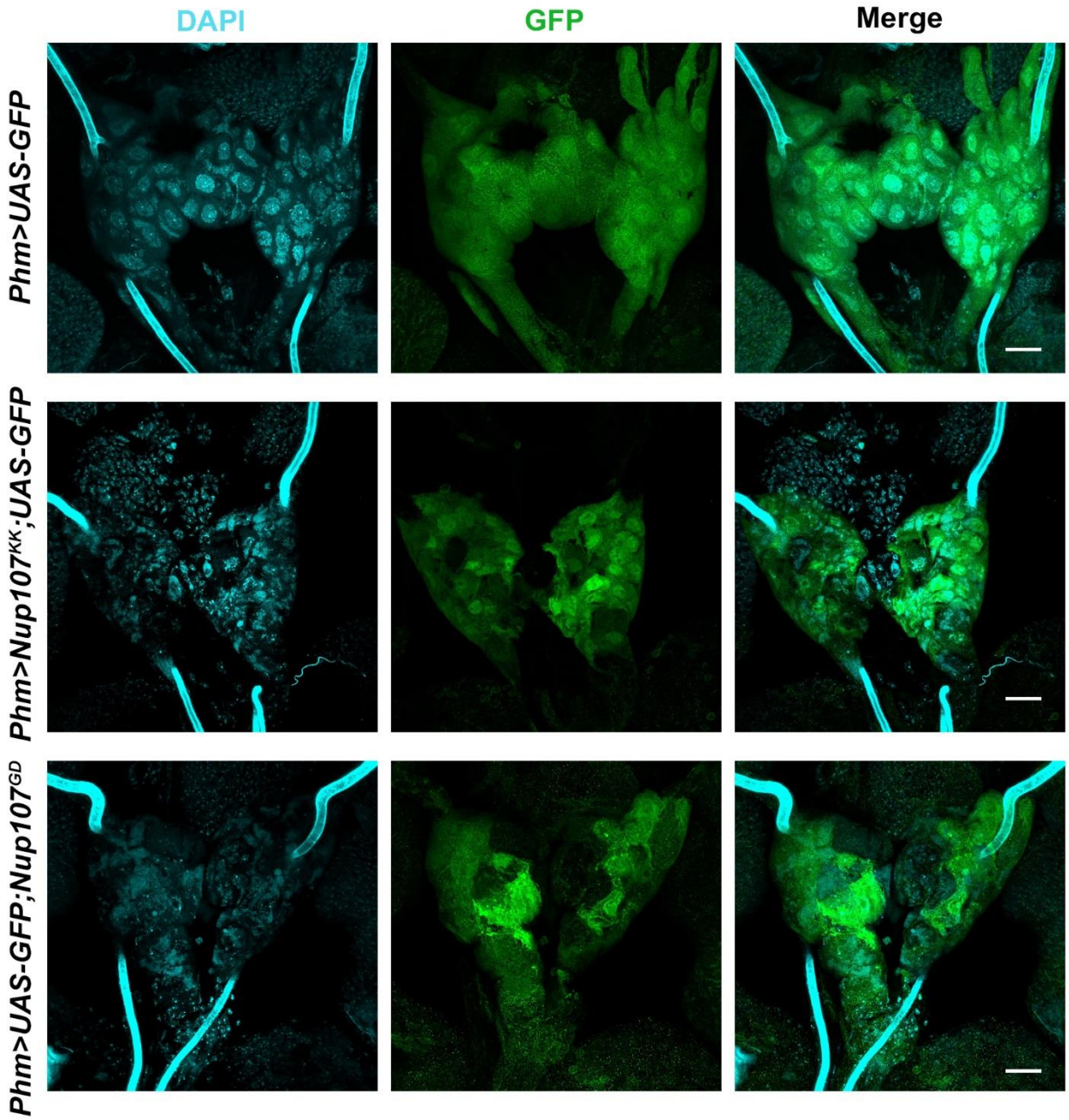

Figure S7. *Nup107* depletion compromises the PG size.

(A-C) Prothoracic gland specific driver *Phm-Gal4* driven expression of GFP in the prothoracic glands of the third instar larva image of Control (A), *Nup107*^{KK} RNAi (B) and *Nup107*^{GD} RNAi (C). DNA stained with DAPI. Scale bars, 20 µm.

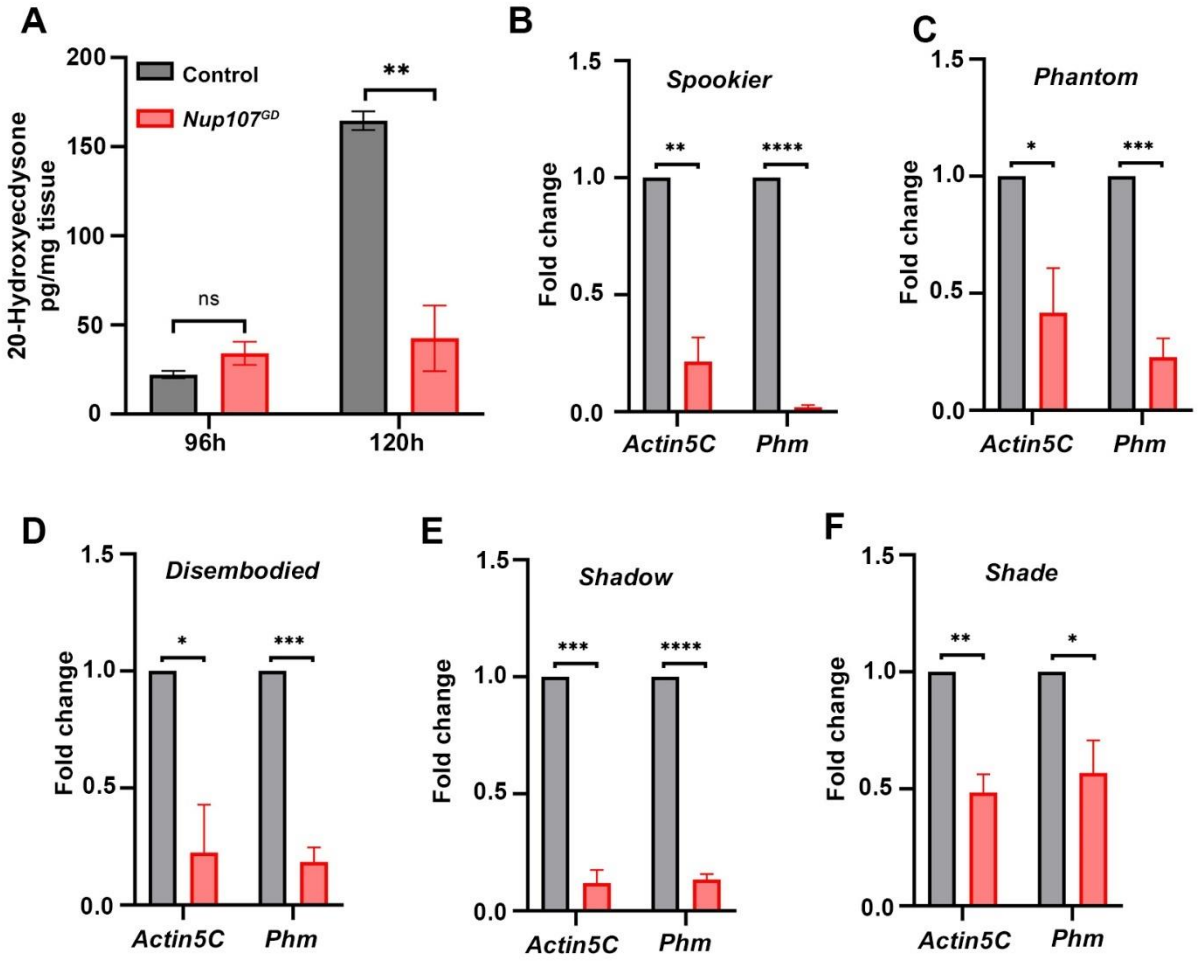

Figure S8. *Nup107^{GD}* RNAi mediated depletion of *Nup107* critically regulates expression of ecdysone-biosynthetic genes:

(A) ELISA measurements of whole-body 20-hydroxyecdysone (20E) levels in control and prothoracic gland-specific (*Phm-Gal4*) *Nup107^{GD}* depletion at 96 and 120 h AEL. Data are represented from at least three independent experiments. Statistical significance was derived from the Student's t-test. Error bars represent SEM. ***p* = < 0.0025 and 'ns' is non-significant.

(B-F) Quantification of ecdysone-biosynthetic gene expression levels of *Spookier* (B), *Phantom* (C), *Disembodied* (D), *Shadow* (E), and *Shade* (F) in cDNA isolated from control, and *Nup107* knockdown late third instar larvae. Data are represented from at least three independent experiments. Statistical significance was derived from the

Student's t-test. Error bars represent SEM. ****p = < 0.0001, ***p = <0.0005, **p = <0.001 and *p = <0.03.

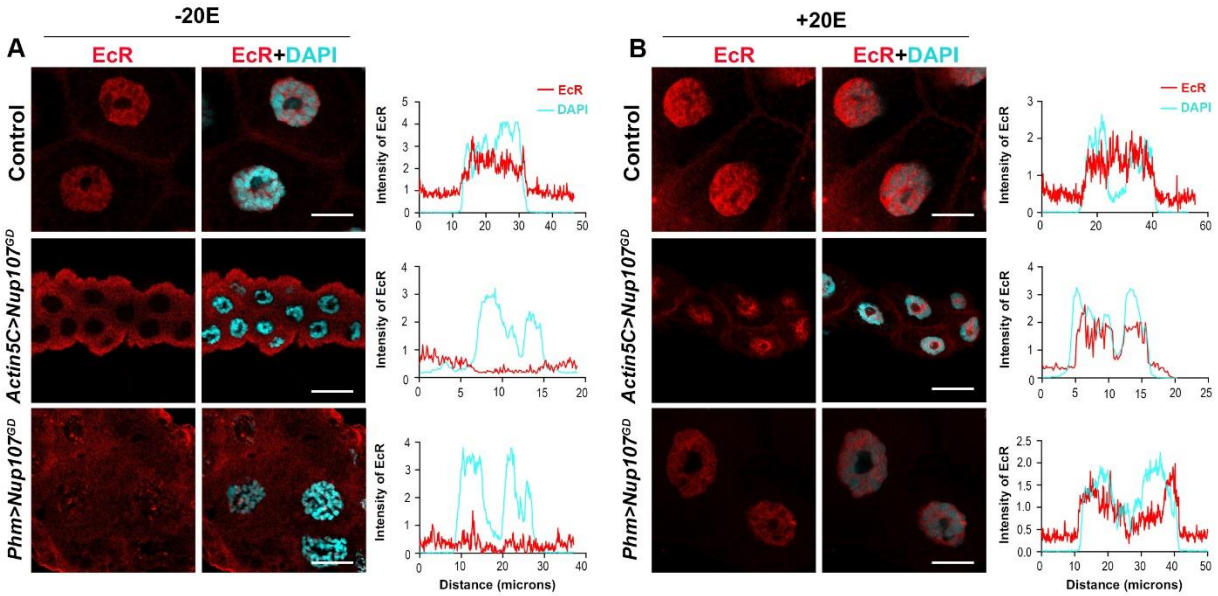

Figure S9. Ecdysone (20E) supplementation rescues *Nup107^{GD} dependent Nup107* depletion specific EcR signaling defects.

(A-B) Visualization of the nucleocytoplasmic distribution of EcR (anti-EcR antibody, red) without 20E (A) and with 20E (B) treatment in larval salivary glands of control, ubiquitous (*Actin5C-Gal4*) *Nup107^{GD}* knockdown, and prothoracic gland-specific (*Phm-Gal4*) *Nup107^{GD}* knockdown. DNA is stained with DAPI. Scale bar, 20 μm. Charts represent the line scan intensity profile of EcR (Red) and DAPI (Cyan) in the salivary gland nucleus region.

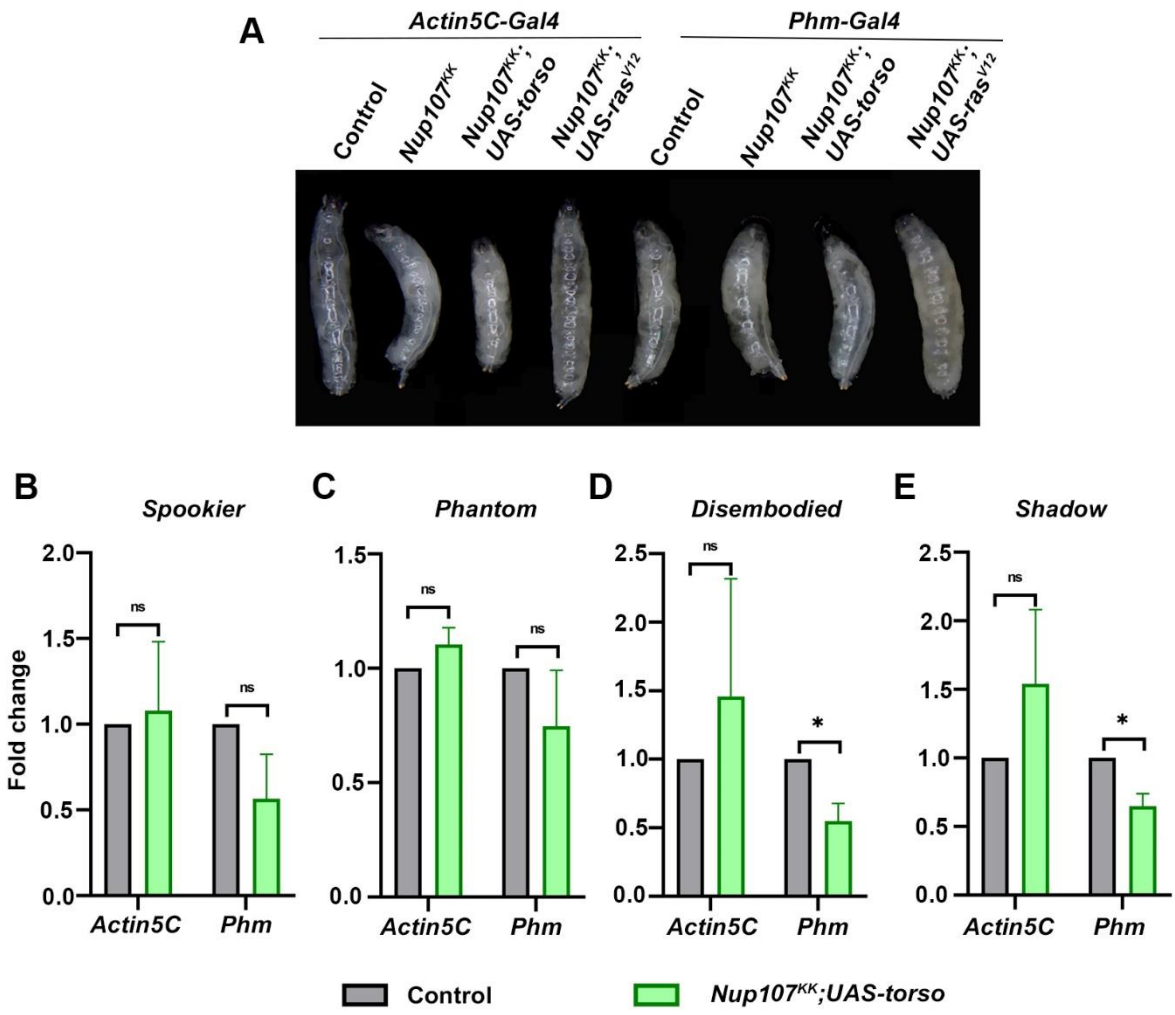

Figure S10. *Torso* rescues metamorphic defects of *Nup107* knockdown:

(A) Growth profile of third instar larvae from different genotypes (Control, *Nup107*^{KK}, *Nup107*^{KK}*;UAS-torso,* and *Nup107*^{KK}*;UAS-ras*^{V12}) at 96 hours AEL (after egg laying).

(B-E) Quantification of ecdysone-biosynthetic gene expression levels of *Spookier* (B), *Phantom* (C), *Disembodied* (D) and *Shadow* (E) in cDNA isolated from control and *Nup107* depleted *torso* overexpressing larvae (by using *Actin5C-Gal4* and *Phm-Gal4*). Data are represented from at least three independent experiments. Statistical significance was derived from the Student's t-test. Error bars represent SEM. (*) represents $p < 0.03$ and 'ns' is non-significant.

Table S1. Exogenous 20E supplementation analysis.

Genotype	-20E	+20E
Control	100%	100%
Phm>Nup107^{KK}	0%	70-80%